

## Review article

Yan-Gang Bi, Jing Feng\*, Jin-Hai Ji, Fang-Shun Yi, Yun-Fei Li, Yue-Feng Liu, Xu-Lin Zhang and Hong-Bo Sun

# Nanostructures induced light harvesting enhancement in organic photovoltaics

<https://doi.org/10.1515/nanoph-2017-0060>

Received June 1, 2017; revised August 29, 2017; accepted September 11, 2017

**Abstract:** Lightweight and low-cost organic photovoltaics (OPVs) hold great promise as renewable energy sources. The most critical challenge in developing high-performance OPVs is the incomplete photon absorption due to the low diffusion length of the carrier in organic semiconductors. To date, various attempts have been carried out to improve light absorption in thin photoactive layer based on optical engineering strategies. Nanostructure-induced light harvesting in OPVs offers an attractive solution to realize high-performance OPVs, via the effects of antireflection, plasmonic scattering, surface plasmon polarization, localized surface plasmon resonance and optical cavity. In this review article, we summarize recent advances in nanostructure-induced light harvesting in OPVs and discuss various light-trapping strategies by incorporating nanostructures in OPVs and the fabrication processing of the micro-patterns with high resolution, large area, high yield and low cost.

**Keywords:** organic photovoltaics; nanostructures and nanomaterials; light manipulation; microstructure fabrication; photons trapping.

## 1 Introduction

Sunlight as an abundant and easily available natural energy resource possesses significant and potential value in dealing with the world energy crisis and greenhouse effect. Photovoltaics is a promising technology to generate electrical power with the conversion of sunlight to electricity on a large scale. In the past decades, organic photovoltaics (OPVs) have attracted considerable research attention because of their unique advantages, such as lightweight, flexibility, semitransparency, low cost and solution processing [1–3]. High power conversion efficiency (PCE) is one of the key considerations for the commercial application of OPVs, for which much attempts have been devoted to developing novel organic and polymer semiconductors and constructing new device structures. To date, the PCE of OPVs is over the 10% efficiency barrier with the development of material engineering for low-band-gap materials [4]. However, compared with the inorganic photovoltaics, the performance of OPVs is still noncompetitive despite the high extinction coefficient of organic semiconductors.

OPVs typically consist of an electron-donor and an electron-acceptor, which are sandwiched between the anode and the cathode. Under illumination, electrons from the highest occupied molecular orbital (HOMO) of the donor are excited to the lowest unoccupied molecular orbital (LUMO) or some higher excited states and then transfer to the LUMO of the acceptor, resulting in separated holes and electrons as shown in Figure 1A [7, 8]. The photocurrent generation by converting solar energy into electrical energy in OPVs can be separated into four key processes as described in Figure 1B: (1) light absorption to excite electron transition and create excitons, (2) exciton diffusion to the interface of the donor and the acceptor and splitting into free carriers, (3) transport of free holes in the donor and electrons in the acceptor owing to the built-in electric field, and (4) collection and extraction of charges by the electrodes [6]. Since the pioneering work of Tang [9], the planar heterojunction (PHJ) structure of photoactive layers with sequentially

\*Corresponding author: **Jing Feng**, State Key Laboratory of Integrated Optoelectronics, College of Electronic Science and Engineering, Jilin University, 2699 Qianjin Street, Changchun 130012, People's Republic of China, e-mail: jingfeng@jlu.edu.cn  
**Yan-Gang Bi, Jin-Hai Ji, Fang-Shun Yi, Yun-Fei Li, Yue-Feng Liu and Xu-Lin Zhang** : State Key Laboratory of Integrated Optoelectronics, College of Electronic Science and Engineering, Jilin University, 2699 Qianjin Street, Changchun 130012, People's Republic of China  
**Hong-Bo Sun**: State Key Laboratory of Integrated Optoelectronics, College of Electronic Science and Engineering, Jilin University, 2699 Qianjin Street, Changchun 130012, People's Republic of China; and Department of Precision Instrument, Tsinghua University, Haidian, Beijing 100084, People's Republic of China

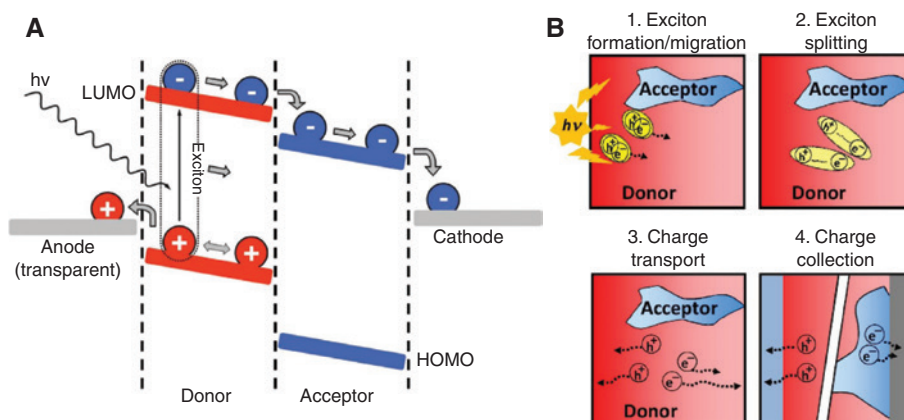


**Figure 1:** Device operating principle of OPVs.

(A) Schematic diagram of the principles of the internal processes in OPVs (reprint with permission Ref. [5]; Copyright 2010 Elsevier Ltd.).

(B) The four processes of photocurrent generation in OPVs (reprint with permission Ref. [6]; Copyright 2015 Elsevier Ltd.).

**Table 1:** The commonly used photoactive systems in OPVs.

Active layer system		Type	LUMO/HOMO (eV)		Thickness (nm)	PCE (%)	Ref.
Donor	Acceptor		Donor	Acceptor			
CuPc	C <sub>60</sub>	PHJ	3.5/5.2	4.5/6.2	35 + 70	1.07	[10]
CuPc	PTCBI	PHJ	3.5/5.2	4.4/6.1	11 + 4	–	[11]
SubPc	C <sub>60</sub>	PHJ	3.5/5.6	4.5/6.3	11 + 45	3.45	[12]
ZnPc	C <sub>60</sub>	BHJ	3.78/5.17	4.5/6.3	35	3.90	[13]
P3OT	C <sub>60</sub>	BHJ	3.0/5.2	4.5/6.3	150	1.1	[14]
TAPC	C <sub>70</sub>	BHJ	1.8/5.5	4.39/6.2	60	4.89	[15]
P3HT	PC <sub>61</sub> BM	BHJ	3.0/4.9	3.70/6.01	210–230	4.37	[16]
P3HT	ICBA	BHJ	3.0/4.9	3.7/5.8	230	5.28	[17]
PBT1	PC <sub>61</sub> BM	BHJ	3.20/4.90	3.70/6.01	~100	4.76	[18]
PBT2			3.22/4.94			5.10	
PBT3			3.29/5.04			5.57	
PBT4			3.31/5.12			3.10	
PBT5			3.24/5.01			3.02	
PBT6			3.17/5.01			2.26	
MEH-PPV	PC <sub>61</sub> BM	BHJ	3.2/5.3	3.70/6.01	80–100	1.89	[19]
PTB7	PC <sub>71</sub> BM	BHJ	3.31/5.15	4.3/6.0	100	7.04	[20]
PBDTTT-E-T	PC <sub>70</sub> BM	BHJ	3.22/5.04	4.3/6.1	100	6.21	[21]
PBDTTT-C-T	PC <sub>70</sub> BM	BHJ	3.25/5.11	4.3/6.1	100	7.59	[22]
PBDTT-DPP	PC <sub>71</sub> BM	BHJ	3.6/5.3	4.3/6.1	100	6.59	[23]
PCDTBT	PC <sub>71</sub> BM	BHJ	3.6/5.5	4.3/6.1	80	6.02	[24]
						1.89	
PFSDCN	PCBM	BHJ	3.25/5.32	3.9/5.9	65	1.64	[25]
DPP(TBFu) <sub>2</sub>	PC <sub>71</sub> BM	BHJ	3.4/5.2	4.0/5.8	100	4.4	[26]
DTS(PTTh <sub>2</sub> ) <sub>2</sub>	PC <sub>70</sub> BM	BHJ	3.6/5.2	4.3/6.1	130–180	6.70	[27]

CuPc, copper (II) phthalocyanine; C<sub>60</sub>, fullerene; PTCBI, 3,4,9,10-perylenetetracarboxylic bisbenzimidazole; SubPc, boron subphthalocyanine chloride; ZnPc, Zinc phthalocyanine; P3OT, poly(3-octylthiophene); TAPC, 1,1-bis-(4-bis(4-methyl-phenyl)-amino-phenyl)-cyclohexane; P3HT, poly(3-hexylthiophene); ICBA, indene-C60 bisadduct; PC<sub>61</sub>BM, [6,6]-phenyl-C61-butyric acid methyl ester; PC<sub>71</sub>BM, [6,6]-phenyl-C71-butyric acid methyl ester; MEH-PPV, poly(2-methoxy, 5-(2'-ethylhexyloxy)-1,4-phenylene vinylene); PBTs, thieno[3,4-b]thiophene and benzodithiophene units; PTB7, poly(3-fluoro-2-[(2-ethylhexyl)carbonyl]thieno[3,4-b]thiophenediyl)); PBDTTT-C-T, poly[[4,8-bis-(2-ethylhexyl-thiophene-5-yl)-benzo[1,2-b:4,5-b']dithiophene-2,6-diyl]-alt-[2-(2'-ethylhexanoyl)-thieno[3,4-b]thiophen-4,6-diyl]]; PBDTT-DPP, poly[2,6'-4,8-di(5-ethylhexylthienyl)benzo[1,2-b:3,4-b]dithiophene-alt-5-dibutyl-3,6-bis(5-bromothiophen-2-yl)pyrrolo[3,4-c]pyrrole-1,4-dione]; PCPDTBT, poly[2,6-(4,4-bis-(2-ethylhexyl)-4H-cyclopenta[2,1-b:3,4-b']dithiophene)-alt-4,7(2,1,3-benzothiadiazole)]; DPP(TBFu)<sub>2</sub>, benzofuran-substituted DPP\_OT\_3,6-bis(5-(benzofuran-2-yl)thiophen-2-yl)-2,5-bis(2-ethylhexyl)pyrrolo[3,4-c]pyrrole-1,4-dione; PFSDCN, poly[2,7-(9,9-dioctylfluorene)-alt-2-((4-(diphenylamino)phenyl)thiophen-2-yl)malononitrile]; DTS(PTTh<sub>2</sub>)<sub>2</sub>, 5,50-bis(4-(7-hexylthiophen-2-yl)thiophen-2-yl)-[1,2,5]thiadiazolo[3,4-c]pyridine-3;30-di-2-ethylhexylsilylene-2;20-bithiophene.

deposited neat donor-acceptor bilayers has been widely used for small molecule-based OPVs. Another type of heterojunction structure commonly used in OPVs is bulk heterojunction (BHJ) by intermixing or blending the donor and acceptor materials. The interpenetrating network of BHJ allows the photogenerated excitons to reach the donor-acceptor interface with high probabilities, and the BHJ is also considered the predominant structure for solution-processed OPVs. The commonly used donor-acceptor systems nowadays based on small molecule or polymer photoactive materials are listed in Table 1 with their work functions, heterojunction structures, thicknesses as well as PCEs.

In conventional OPVs, because of the intrinsically high exciton binding energy, short exciton diffusion length and low charge mobility of organic materials, the thickness of the photoactive layer is commonly around 100 nm for efficient electron and hole dissociation and transport [28–30]. The thickness of the photoactive layer is far less than the optical absorption length of organic semiconductors, and a large fraction of incident photons remain unabsorbed. The incomplete light absorption in the thin photoactive layer limits the external quantum efficiency of OPVs. In order to remit the conflict between optical absorption length and carrier diffusion length in OPVs, sophisticated polymers with high carrier mobilities were developed to improve charge dissociation and transport in thick active layers [31–33].

Optical manipulation inside OPVs by incorporating nanostructures provides an alternative method to enhance light trapping and boost the efficiency of OPVs. A variety of strategies with distinct mechanisms have been reported in recent years to realize significant light harvesting induced by nanostructures in OPVs. On the one hand, introducing an out-of-cell antireflective microstructure on the front side of the substrate or transparent electrode is a direct method to enhance light harvesting via reducing the reflective losses [34]. On the other hand, light is concentrated and amplified in the photoactive layer by integrating in-cell nanostructures as well as nanomaterials combined with optimizing device construction. Plasmonic in-cell nanostructures have been investigated comprehensively in OPVs, and the incident light can be effectively trapped and coupled inside photoactive layers via metal nanostructures or nanomaterial-induced plasmonic scattering, surface plasmon polariton (SPP) effects and localized surface plasmon resonance (LSPR) effects [35–38]. Constructing OPV devices with microcavity, optical spacer and distributed Bragg reflectors can optimize the optical field distribution and improve the efficiency of OPVs [39, 40]. The aim of this article was to review optical

engineering strategies in OPVs to realize the nanostructure-induced light harvesting. The effects and schemes of the nanopattern-induced light manipulation inside photoactive layers as well as the fabrication technique of nanostructures in the OPVs will be discussed.

## 2 Fabrication technologies for nanostructures

The structural parameters of nanostructures play important roles in light manipulation to excite, trap and couple photons in optical modes. The availability of inexpensive and scalable micro- and nano-fabrication technologies with high resolution is a key to the commercial adoption of OPVs. Although electron beam lithography (EBL) and focused ion beam lithography have been used for the mass production of nanostructures with high resolution, real-world application in large-scale photovoltaic module is impractical. In this section, we will discuss some novel micro- and nano-fabrication technologies to form versatile and scalable patterns in OPVs, including laser-assisted fabrication, nanoimprint lithography (NIL) and self-assembled process.

### 2.1 Laser-fabricated periodic nanostructures

The laser-assisted process is one of the most promising technologies for microstructure fabrication, such as femtosecond laser direct writing, owing to its high fabricating resolution, three-dimensional (3D) fabricating capability and flexible designability for micro- or nanostructures [41–43]. The holographic lithography technique based on laser beam interference with high controllability and reproducibility is commonly used to obtain periodic nanostructures. Figure 2A shows the schematic diagram of the holographic lithography process [44]. The periodically changed light field intensity arising from two laser beam interference can be recorded by the photoresist film spin coated on the substrates during the exposure process, and periodic nanostructures can be obtained after dipping the exposed photoresist film in a developing solution. The period is regulated by the laser wavelength and the angle of the interference beams, and the amplitude and space ratio are controlled by the exposure time and laser fluence. Dual periodic nanostructures have also been reported on the basis of the holographic lithography technique with the twice-exposure process, and the sample was

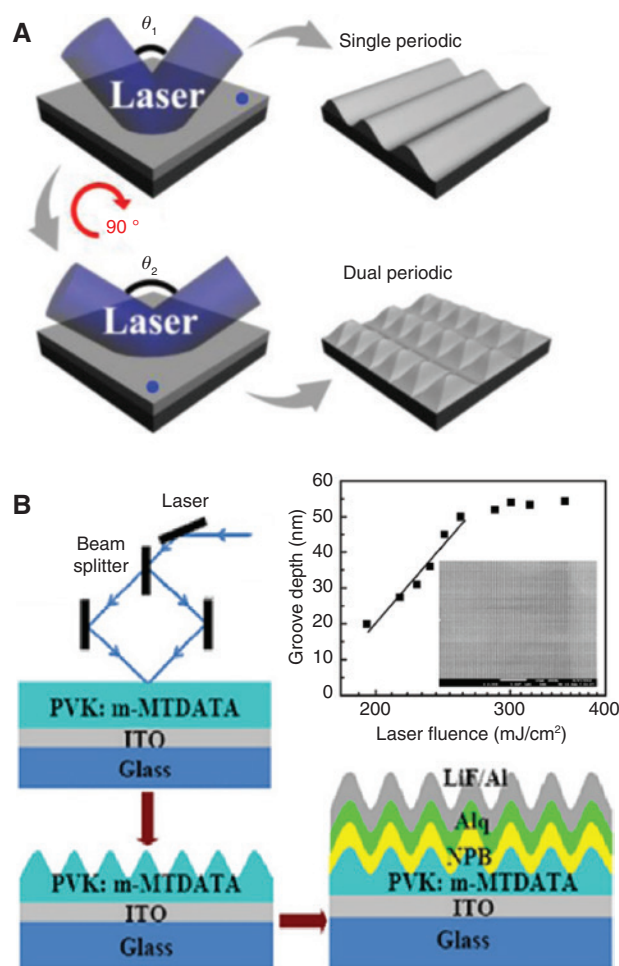


**Figure 2:** Two-beam interference lithography technique. (A) Schematic diagram of holographic lithography process (reprint with permission Ref. [44]; Copyright 2015 Elsevier B.V.). (B) The schematic diagram of introducing periodic microstructure directly into the organic functional layers by laser ablation. The inset shows the etch depth by one pulse laser ablation as a function of the laser fluence (reprint with permission Ref. [45]; Copyright 2011 Elsevier B.V.).

exposed for the second time with different writing periods and intersection angles [46].

Most materials used in OPVs are sensitive to ultraviolet (UV) laser ablation condition, so that periodic nanostructures can be directly fabricated on the organic functional layers in OPVs via laser ablation by the two-beam interference lithography technique. Figure 2B shows a periodic one-dimensional grating recorded on a poly(N-vinyl carbazole) (PVK) film as the corrugated hole transport layer, and the relationship of groove depth and laser power has been investigated as shown in the inset of Figure 2B [45]. A linear dependence of the groove depth on the logarithm of the laser fluence at low energy density is demonstrated, and a deviation at high laser fluence can also be found due to the limitation of the film thickness.

By combining two-beam interference lithography with angle-multiplexed exposure processing, the large-area multiscale hierarchical structures with 3D surface profiles have been printed (Figure 3A), which have comparable aspect ratios with periods ranging from 300 nm to 4  $\mu\text{m}$  and amplitudes ranging from 40 to 900 nm, respectively [47]. Various complex functional nanostructures can be rapidly realized by multibeam laser interference lithography. Figure 3B shows S-shaped and chain-like nanostructures as well as pillar-cell arrays fabricated by controlling the widths and heights of the pillars prepared by multibeam laser interference lithography [48].

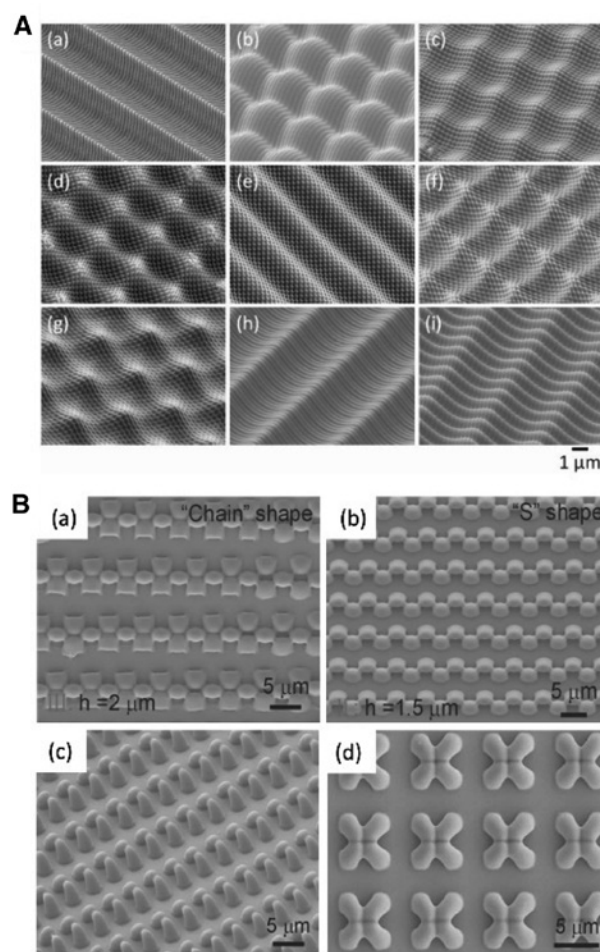


**Figure 3:** Angle-multiplexed optical imprinting and multibeam laser interference lithography. (A) Scanning electron microscopy (SEM) images of multiscale hierarchical structures fabricated by two-beam interference lithography in combination with angle-multiplexed exposure processing (reprint with permission Ref. [47]; Copyright 2017 WILEY-VCH Verlag GmbH & Co. KGaA, Weinheim). (B) SEM images of S-shaped, chain-like, two-pillar-cell and four-pillar-cell arrays fabricated by multibeam laser interference lithography (reprint with permission of Ref. [48]; Copyright 2013 Wiley-VCH Verlag GmbH & Co. KGaA, Weinheim).

## 2.2 Template-assisted fabrication method

Imprint processing is a fabricating technology for embossed structures based on the physical modeling method and transfers the embossed templates to the surface of samples [49, 50]. NIL with high resolution, excellent yield and low cost was first developed by S. Chou from the University of Minnesota in 1995 [51]. The NIL technology avoids the light diffraction in optical lithography and can fabricate the nanoscale structure with fabricating accuracy up to several nanometers [52]. In the fabrication of nanoscale embossing templates, which play major roles in NIL, high-resolution reactive ion etching (RIE) and EBL are usually applied [53]. Thermal NIL is an earlier developed nanoimprinting technology, and nanostructures are directly formed onto a heated or molten thermal substrate material surface over its glass transition temperature ( $T_g$ ) under a certain pressure as shown in Figure 4A [55]. The heating and cooling processes in thermal NIL increase the stamping cycles, as well as the wastage of templates. In the development of imprint processing, various low-temperature NIL technologies have sprung up, such as UV-curable NIL (Figure 4B) [56, 57]. Instead of thermal pressing formation, the microstructured polymers form at room temperature by UV exposure polymerization with additives as UV photoinitiators, which enable high-speed, large-scale and high-throughput microstructure fabrication.

Thermal NIL and UV-curable NIL are more or less followed by additional processes for further pattern transferring or etching to remove residual materials in hot or UV embossing. Micro/nano-contact NIL has been reported as an alternative for thermal and UV-curable nanoimprint, and ink materials on the template were directly transferred onto uneven surfaces and plastic sheets with designed patterns as shown in Figure 4C [58, 59]. The printed ink materials range from polymer solution, living cells, DNA molecules to metallic films. New endeavors have been done in NIL development for high-speed and large-area patterns, such as roll-to-roll nanoimprint, which is the scale-up development of NIL technology for large-area and high-yield microstructure formation with nanoscale resolution [54, 60, 61].

## 2.3 Self-assembled nanostructures

The thermal annealing process is commonly used to fabricate self-assembled nanostructures, such as buckling structures and wave-like patterns [62, 63]. A range of self-assembled nanostructures induced on the surface of elastomeric polymer films by the stress relief of thin films under internal compressive stress, which have been used in biological, mechanical and physical fields including optical and electronic devices [64–67]. Figure 5 shows the schematic illustration of the fabrication of self-assembled

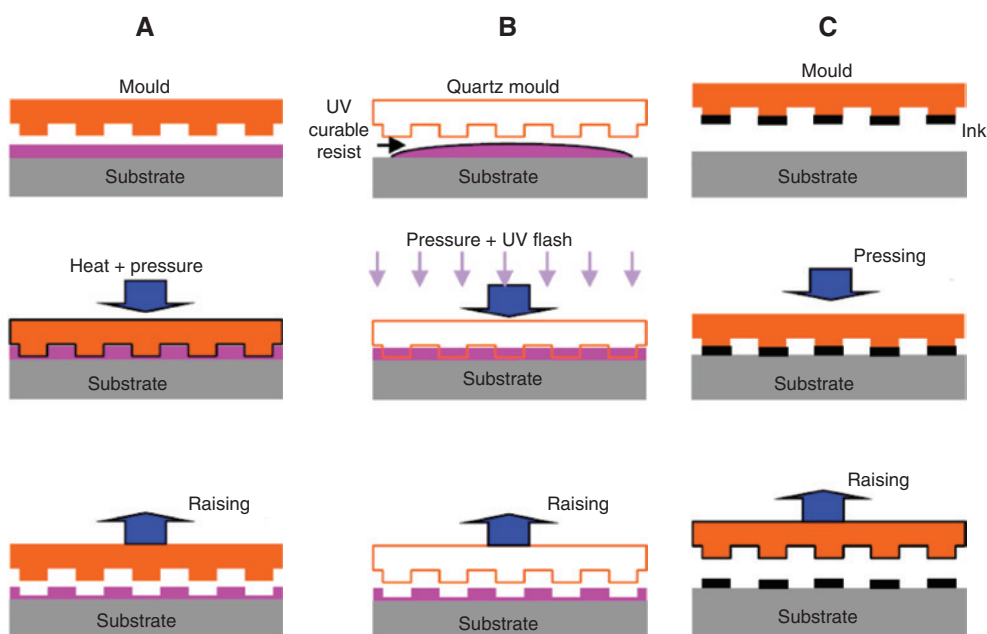


**Figure 4:** Nanoimprint lithography technology.

Schematic diagram of technological processing of (A) thermal NIL, (B) UV-curable NIL and (C) micro/nano-contact NIL (reprint with permission Ref. [54]; Copyright 2015 Springer-Verlag Berlin Heidelberg).

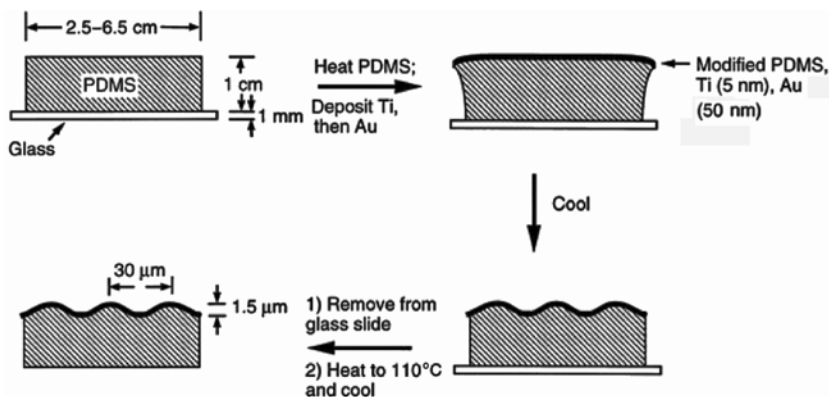


**Figure 5:** Schematic illustration of the fabrication of self-assembled nanostructures (reprint with permission Ref. [68]; Copyright 1998, Rights Managed by the Nature Publishing Group).

nanostructures with the thermal annealing process. Wave-like patterns are introduced spontaneously by thermally depositing Ti and Au films on preheated polymer substrates (PDMSs) [68]. After cooling to room temperature, wave-like nanostructures spontaneously occurred to release the internal compressive stress arising from the difference between the thermal expansion coefficients of the PDMS and the deposited metal film. The depths and quasi-periods of nanostructures depend on the imposed compressive strains which are proportional to the thickness of the thin films and annealing temperature as well as annealing time [69]. The orientations of the surface self-assembled patterns have a strong dependence on the surface morphology of polymer films, and the spontaneous formation of complex ordered nanostructures has been reported on the photochemistry patterned elastomeric polymer surface [68, 70, 71].

The thermal annealing method has also been employed to obtain metal nanoparticles (NPs) in OPVs to excite LSPR or plasmon scattering [72–74]. The particles can be directly deposited and spontaneously fabricated on the indium tin oxide (ITO) anode by the thermal annealing process, which is favorable for their application in OPVs. The Au-Ag alloy NPs in OPVs have been reported by the co-evaporation of Au and Ag onto the ITO substrate followed by the thermal annealing process, and the atomic composition of the alloy NPs was controlled by tuning the deposition rate of the Au and the Ag [75]. Mallik et al. demonstrated a UV-photoactivation technique to prepare bimetallic Au and Ag NPs with a core-shell-type structure. Initially, Au particles as the seed particles catalyzed and mediated the reduction of the added silver ion in the presence of UV light to yield bimetallic  $\text{Au}_{\text{core}}-\text{Ag}_{\text{shell}}$  NPs [76]. Metal nanomaterials, including metal NPs, bimetallic NPs and alloy NPs, can also be fabricated by chemical

synthesis with a wide range of sizes, shapes and high yields [77–80].

### 3 Nanostructures modulate light harvesting in OPVs

#### 3.1 Nanostructures improve light incidence

Incident light traverses the glass substrate, and transparent or semitransparent electrode and photons are absorbed ultimately by the thin active layer in OPVs. Incident photon absorption can be effectively enhanced by introducing microstructure on the front surface of OPV devices along the incident direction, including gratings, self-assembled nanoholes, random scatters, apertures, microlenses and refractive structures [81–85]. The proposed nanostructures with optimized geometric parameters can reduce the reflection loss of the incident photons, increase the optical path length and enhance the incoupling efficiency in OPVs.

For example, Janssen et al. [81] have applied a polymeric retroreflective textured sheet onto the backside of the glass substrate in OPVs. The retroreflective textured sheet consisted of an array of tilted cubic structures with hundreds microscale as shown in Figure 6A, which was fabricated from a cross-linked poly(dimethylsiloxane) (PDMS) using a replication technique with a metal mold. The incident light was scattered and refracted by the textured sheet, and an improved optical path length inside the solar cell was obtained. The fraction of reflected light at the substrate-ITO interface as well as the back reflected light in OPVs was reflected back to the photoactive layer

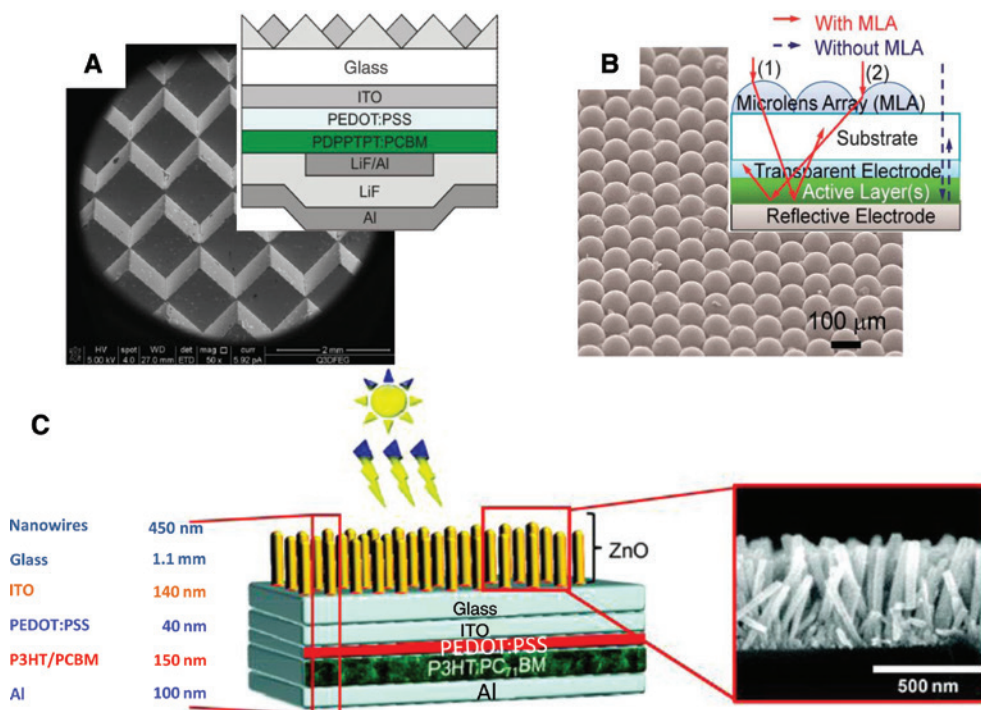


**Figure 6:** Nanostructures improve light incidence.

(A) SEM image of the retroreflective light-trapping texture, and inset shows the device structure (reprint with permission Ref. [81]; Copyright 2013 Wiley-VCH Verlag GmbH & Co. KGaA, Weinheim). (B) SEM image of microlens array, and inset shows the schematic illustration of light trapping with the microlens array (reprint with permission Ref. [86]; Copyright 2012 The Royal Society of Chemistry). (C) Structure of OPVs with ZnO NWs, and SEM image of ZnO NWs (reprint with permission Ref. [87]; Copyright 2014 The Royal Society of Chemistry).

by the polymeric retroreflective textured sheet. Owing to the geometry of the texture effectively capturing the light inside OPVs, the absorption properties of OPVs were improved and the PCE was increased by 19%.

A microlens array incorporated on the incident surface of the glass substrate in an organic-based photovoltaic cell has been reported to enhance light absorption [86]. The closed-packed, transparent, hemispherical microlens array was fabricated by PDMS using a soft-NIL technology and provided an additional angular component for the incident light to increase the path length in the active layer as shown in Figure 6B. The light harvesting introduced by the microlens array has been demonstrated on small molecule-based planar OPVs, BHJ OPVs and polymer-colloidal nanocrystal hybrid OPVs.

Recently, Hiralal et al. [87] proposed OPVs with ZnO nanowires (ZnO NWs) grown on the backside of a glass substrate to improve the performance of OPVs as shown in Figure 6C. The ZnO NWs were used as the antireflection coating to improve light distribution in photoactive layers based on P3HT:PC<sub>71</sub>BM and improved the efficiency by 36%. More interestingly, because of the sufficient absorption in the UV region, ZnO NWs also acted as the UV barrier to reduce the rate of degradation of OPVs and

improve the cell lifetime. The absorbed UV light generated charge carriers in ZnO NWs to form a superhydrophobic surface with self-cleaning function via the Lotus effect. The ZnO NWs with the effects of antireflection, UV barrier and self-cleaning in OPVs revealed potential applications such as in architecture or automobile windows.

### 3.2 Plasmonic effect enhances light trapping

Plasmonic nanostructures, such as periodic metal gratings [88–90], metal NPs [91–94], random corrugations [95–97] and biomimetic structures [98–100], have been investigated universally involving light concentration and manipulation in OPVs. Various kinds of plasmonic nanostructures can effectively trap light inside the photoactive layer owing to the excitation of the surface plasmonic effect, which is the collective oscillations of conductive electrons at the metal/dielectric interface. In general, the plasmonic light-trapping mechanism induced by nanostructures can be concluded to three main modes as shown in Figure 7 [37, 101]. One of the plasmonic light-trapping modes is plasmonic light scattering. The embedded plasmonic nanostructures at the

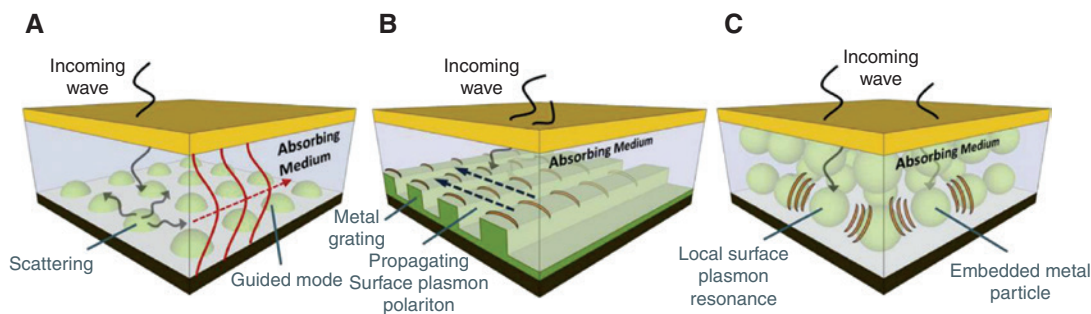


**Figure 7:** Plasmonic light-trapping mechanism in OPVs based on plasmonic nanostructures.

(A) Plasmonic light scattering, (B) SPP effect and (C) LSPR effect (reprint with permission Ref. [101]; Copyright 2011 Materials Research Society).

interface of the OPVs, such as metal NPs, scatter the incident light into the devices with an additional angular spread, and the photons are then trapped partially in the thin absorber films by the reflection between back metal electrodes and microstructured interfaces, resulting in an increased effective path length inside OPVs. The second mode of plasmonic light trapping is the SPP mode. Effective light trapping is realized due to the optical coupling at the corrugated metal-organic interface associated with the excitation of SPP modes. The third mode of plasmonic light trapping is the LSPR effect. Metal NPs inside the absorbing medium act as the subwavelength antennas to concentrate the optical field and increase the effective absorption cross-section. In the following section, we will discuss these plasmonic light-trapping modes as well as the design of OPV constructions based on plasmonic nanostructures in detail.

### 3.2.1 SPPs

SPPs are guided electromagnetic waves traveling along the interface between a metal and a dielectric film [102–104]. By introducing a microstructured metal/dielectric interface to surmount the mismatch associated with the momentum of in-plane SPPs and incident photons, the SPP modes can be excited and the incident photons will be trapped and guided along the interface for a few micrometers until the energy is lost in metal and dielectric materials. The incident solar flux is transferred perpendicular to the incident direction and absorbed by the photoactive materials nearby the microstructured interface [105–108]. Forrest et al. [108] have fabricated periodic 1-D metallic grating at the submicron scale based on nanolithography and explored their application in OPVs based on a small molecular active layer. Baba et al. have engaged 1-D Ag grating to excite the SPP mode associated with the cathode interface and realized a twofold improvement in

photocurrent in OPVs based on the solution-processing P3HT:PCBM photoactive layer [88].

The optical effects of periodic metal nanostructures for light harvesting and device performance improvement in OPVs have been demonstrated by the theoretical simulation based on the finite-difference time domain (FDTD) method. In the simulated distribution of the magnetic field intensity in the corrugated OPVs with a period of 200 nm under normal incidence at the 450-nm wavelength (Figure 8B), the field intensity showed the maximum value at the corrugated metal/organic interface and delayed along the direction perpendicular to it, which demonstrated the excitation of the SPP modes and light trapping associated with the corrugated interface [44]. The geometrical parameters of the periodic metallic gratings determine the resonance frequency and coupling efficiency of the exciting SPP modes. Figure 8C shows the absorption spectra of the OPVs based on the CuPc/C<sub>60</sub> heterojunction with various periodic Ag gratings, quoted from Jin Yu's work, and multifarious absorption enhancements were obtained associated with the different periods [10]. The optimized improvement for efficiency was realized with the consistent wavelength region between the photoactive absorption and the excited SPP mode resonance in periodic nanostructure-based OPVs.

The main obstacle for the 1-D periodic microstructure-induced light amplification in OPVs is the unequal light trapping of transverse magnetic (TM) and transverse electric (TE) polarized modes due to the sensitive light polarization dependence of the 1-D periodic grating, and only the TM polarized mode with a magnetic component parallel to the 1-D periodic grating can couple to the SPP mode [111]. In addition, the resonance wavelength of the SPPs is relatively narrow compared with the broadband solar light, which is limited by the intrinsic dispersive metal properties and significantly depends on the incident light angle [112]. The polarization dependence and narrow resonance of the SPP modes hinder the application of the

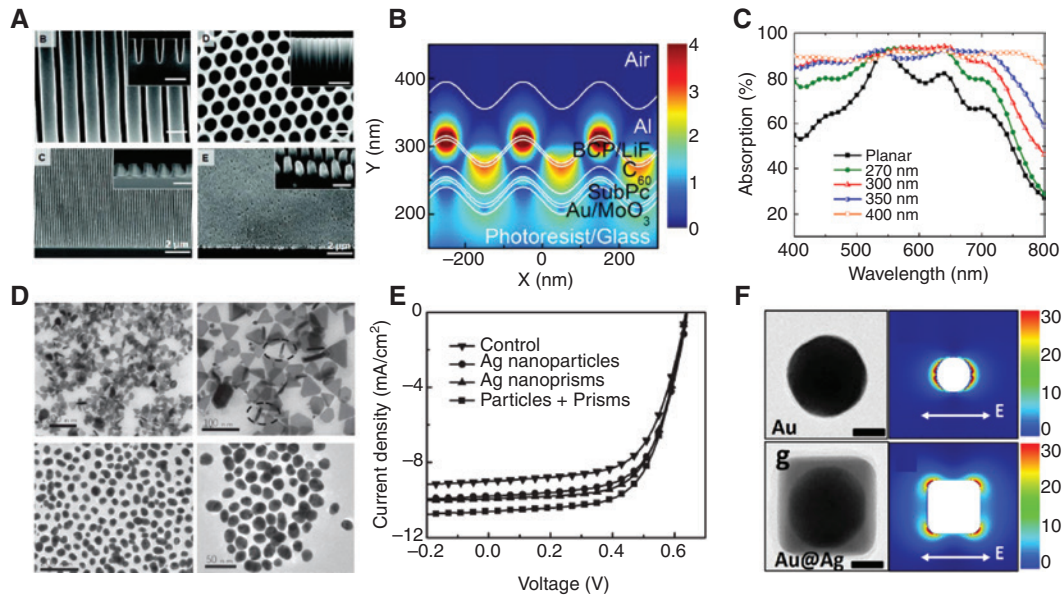


**Figure 8:** Nanostructures enhance light trapping based on plasmonic effect.

(A) SEM images of 1-D and 2-D periodic gratings (reprint with permission Ref. [109]; Copyright 2009 American Chemical Society). (B) Simulated distribution of the magnetic field intensity in the corrugated OPVs at the wavelength of 450 nm based on 200-nm periodic Al cathode, and the device structure can also be obtained in the figure (reprint with permission Ref. [44]; Copyright 2015 Elsevier B.V.). (C) Simulated absorption spectra of OPVs based on CuPc/C<sub>60</sub> heterojunction with 270-, 300-, 350- and 400-nm periodic Ag grating (reprint with permission Ref. [10]; Copyright 2012 American Institute of Physics). (D and E) Transmission electron microscopy (TEM) images of spherical Ag NPs and triangular Ag nanoprisms, and *J-V* characteristics of OPVs with and without metal NPs (reprint with permission Ref. [92]; Copyright 2013 Wiley-VCH Verlag GmbH & Co. KGaA, Weinheim). (F) TEM images of AuNPs and Au@Ag NCs (scale bar: 20 nm), and simulated electric field  $|E|^2$  distributions of AuNPs (45 nm) and Au@Ag NCs (45 nm @ 10 nm) (reprint with permission Ref. [110]; Copyright 2014 American Chemical Society).

1-D periodic nanostructures in OPVs. The introduction of 2-D periodic metal corrugations as the replacement of 1-D grating in OPVs is an effective approach to overcome the deficiencies mentioned above [113]. Benefiting from the geometric symmetries associated with the different in-plane directions, both the TM and TE polarized modes can couple to the SPP modes. Kim et al. [114] have explored the polymer-based BHJ OPVs with 1-D and 2-D gratings. The P3HT:PCBM-based OPVs integrated with the 2-D grating demonstrated a higher enhancement factor compared with the 1-D microstructured devices. The short-circuit current density ( $J_{sc}$ ) and PCE under one sun with AM 1.5 G illumination were improved from 9.5 mA/cm<sup>2</sup> and 3.6% for the planar reference cells to 10.5 mA/cm<sup>2</sup> and 4.1% for 1-D grating-based cells, and to 10.9 mA/cm<sup>2</sup> and 4.3% for 2-D grating-based cells. In order to broaden the light-trapping region, we have designed a 2-D dual-periodic corrugation, which consisted of two sets of different periodic gratings [44]. By tuning the periods of the 2-D dual-periodic corrugation to excite SPP modes according to the absorption wavelength of the donor and acceptor materials, respectively, broadband light trapping has been realized. Atwater and Polman [37] have proposed plasmonic tandem geometries, which may realize broadband light

harvesting as well. The plasmonic tandem geometries included semiconductors with different bandgaps stacked with each other and separated by microstructured metal contact layers with different periods. The independent periodic metal contact layers coupled different spectral bands in the solar spectrum into the corresponding sub-absorber cells in the tandem geometries.

Integrating random corrugations or biomimetic structures with quasi-periodic or random geometry in OPVs is another important and effective means to realize broadband polarization-insensitive light harvesting owing to the excitation of broadband and hybrid SPP modes, such as quasi-grating [115], deterministic aperiodic nanostructures (DANs) [116], porous nanocolumnar [100], bioinspired moth's eye nanostructures (MENs) [99, 100, 117] and ripple structures [118]. For instance, Tang et al. have experimentally and theoretically investigated the random biomimetic structures in OPVs. They proposed DANs and MENs in OPVs to guide and retain light inside the active layer [99, 116, 117]. Moreover, they introduced the DNA and MEN structures onto the backside of glass substrates to reduce reflection losses of the incident light. Owing to the collective effects of the nanostructure-induced broadband SPP excitation, light scattering and antireflection, the broadband absorption

and device performance were significantly improved in OPVs based on dual-side DANs or MENs.

The plasmonic metallic nanostructures also have electrical effects on the performance of OPVs. The parasitic Ohmic loss occurring upon the excitation of surface plasmons is often a common problem when employing metallic nanostructures for OPV applications. Interestingly, it has been reported that the 1-D metallic grating on the back electrode improved the fill factor (FF) of OPVs, which is considered to result from the larger corrugated interfacial area as compared with planar devices as well as the lower series resistance of the nanostructured OPVs [119]. The molecular orientation or crystallinity effects arising from directly imprinting the active layer could give rise to increased charge mobility in the active layer, thereby reducing bulk recombination and series resistance [120]. A recent research has demonstrated that the space charge limit in OPVs could be overcome in OPVs on the basis of metallic grating. This was attributed to the plasmonic nanostructures causing a redistribution of the local exciton generation in the photoactive layer, thus giving a shortened transport path for positive charge carriers in OPVs [121].

### 3.2.2 LSPR

Metal NPs have been used in OPVs to improve efficiency, commonly owing to its relatively simple fabrication process and compatibility with OPVs [122–124]. Metal NPs implanted in photoactive layers can concentrate incident light and store energy to LSPR based on plasmonic near-field coupling [125]. The material, shape, size, concentration, composition and location of incorporated metal NPs are key parameters to tailor the resonant frequency and coupling efficiency of LSPR in OPVs. For example, Guo et al. [126] reported the application of Au arrowhead nanorods (ARNRs) in the inverted polymer OPVs based on PCDTBT and PC<sub>71</sub>BM, and the PCE was improved from 5.75% to 7.40% with a maximum enhancement of 28.7%. Except for exciting the LSPR, the ARNRs in the active layers also reduced the cell resistance and improved the charge transport as demonstrated by the experimental and theoretical analyses. Xu et al. [75] have employed Au-Ag alloy NPs in OPVs and realized tunable LSPR by varying the molar ratio of alloy NPs. A 19% enhancement was obtained by tailoring the LSPR resonant peak in accordance with the absorption of the P3HT:PCBM photoactive layer.

Choy et al. [92] demonstrated broadband light trapping in OPVs with multi-plasmonic-resonant absorption peaks based on metal NPs. They incorporated Ag NPs and nano-prisms with different shapes synthesized by a wet chemical

method in P3HT:PCBM photoactive layers as shown in Figure 8D and E, and low-order and high-order plasmonic resonance modes were excited simultaneously in broadband. Benefitting from the incorporation of LSPR effects excited by the mixed plasmonic Ag nanomaterials, the  $J_{sc}$  was improved by 17.91% and the PCE was increased by 19.44%, as compared to the pre-optimized control sample.

It is worth noting that some detrimental effects exist at the interface between the embedded metal NPs and the organic semiconductors, including the quenching of excited states, non-radiative decay and charge-carrier recombination, which offset the gains from local field enhancement and attenuate the efficiency of OPVs [127–129]. Packing the metal NPs inside an inert cladding layer with core-shell nanostructures to separate from the surrounding semiconductors is an effective approach to reduce the detrimental effects mentioned above. In this regard, Sun et al. [130] have explored the electric function of the ultrathin oxide coating layer on Ag nanoprisms (Ag@TiO<sub>2</sub>). The photoluminescence (PL) quench and the relatively short-lived photon-induced polaron were discovered in cells based on bare Ag nanoprisms owing to the exciton recombination and the quenching of excited states. On the contrary, in the cells with Ag@TiO<sub>2</sub> core-shell nanostructures, an improved photon-induced exciton population was observed from the enhanced absorption and PL spectra as well as the long-lived photon-induced polaron, and a 31% enhancement of PCE was obtained finally due to the LSPR effects of NPs and the protective effects of the oxide shell.

Despite the detrimental effects, the metal nanomaterials in OPVs also have positive electrical effects on the processes of charge-carrier transformation and collection. Borchert et al. [127] have demonstrated that Au NPs incorporated in the photoactive layer increased the performance of OPVs due to the introduction of dopant states, which increased the electrical conductivity of the photoactive layer. Choy et al. [131] have found electrical properties of increased hole mobility and better balance of electron and hole mobilities by incorporating Au NPs into active layers, and increased  $J_{sc}$  and FF were obtained. In addition, the metal nanomaterials incorporated into the buffer layers have demonstrated to be beneficial for extracting the charge carriers from the photoactive layers to the respective electrodes [132].

### 3.2.3 Plasmonic light scattering

Subwavelength NPs located outside the photoactive layer can scatter and trap photons inside the cells. The NPs on

the top of the absorber layer provide a far-field effect to trap light, which is similar in nature to scattering into quasi-guide modes based on the dielectric structure. Owing to the plasmonic light scattering, the NPs with a high scattering cross-section can reduce the reflective losses and provide an enhanced effective path length to increase light incoupling efficiency [133–136]. Plasmonic scattering efficiency can be tailored by the shape, environment, distribution and size of NPs. An 18% enhancement in PCE for PCDTBT:PC<sub>71</sub>BM-based OPVs has been reported by Jung et al. [137] owing to the plasmonic scattering of Ag NPs embedded in the ITO and MoO<sub>3</sub> interface. Au@Ag core-shell nanocubes were incorporated in OPVs to improve plasmonic scattering as shown in Figure 8F, as reported by Baek et al. [110]. The well-manipulated Au@Ag core-shell nanocubes exhibited outstanding scattering efficiency at the long-wavelength region, resulting in a 2.2-fold absorption enhancement compared with the Au NPs.

NPs located at the back of the devices also show comparable scattering efficiencies to those at the front of the devices, which can avoid losses due to the destructive interference between scattered and unscattered light

[138–140]. For instance, Kymakis et al. [141] have reported the plasmonic backscattering effect in OPVs with Au nanorods. Au nanorods inside the electron transport layer (the titanium suboxide, TiO<sub>x</sub>) were demonstrated to provide light trapping via scattering and avoid the optical losses of light back scattering in a front-type plasmonic device. In addition, by placing the NPs on the rear of OPVs, the potential absorption losses in the NPs were also suppressed. As a result, the PCE of PCDTBT:PC<sub>71</sub>BM-based OPVs and PTB7:PC<sub>71</sub>BM-based OPVs was improved by 13% and 8%, respectively.

### 3.2.4 Dual plasmonic effects

SPPs excited by periodic metal gratings and LSPR induced by metal NPs typically have relatively narrow and different resonance wavelength regions [142–144]. It is interesting to simultaneously extend the wavelength region of light trapping in OPVs based on SPPs and LSPR. Choy et al. and Yang et al. designed inverted OPVs based on dual plasmonic nanostructures, as shown in Figure 9,

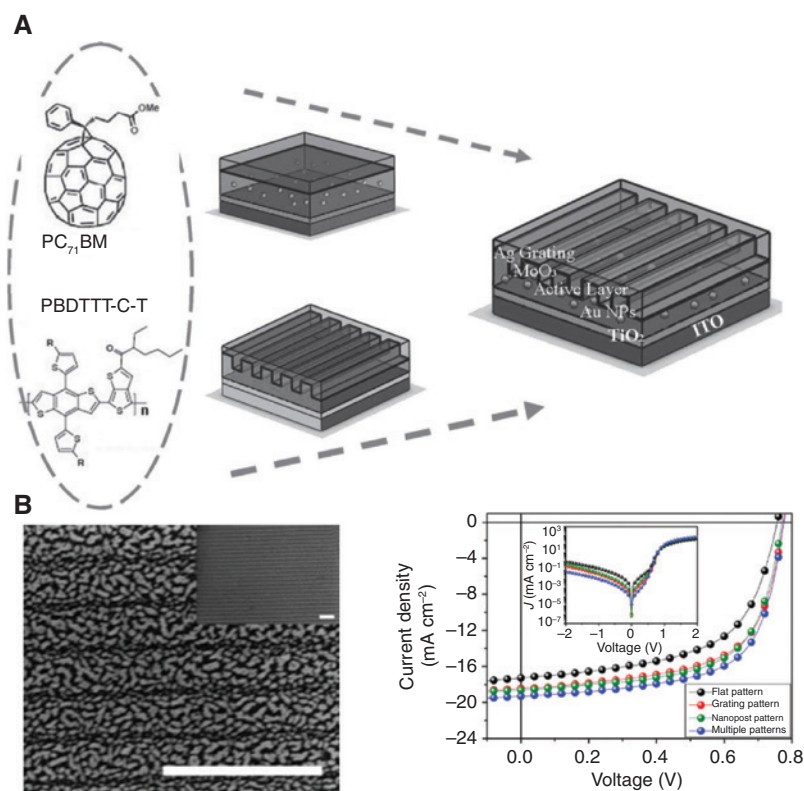


**Figure 9:** Dual plasmonic effects enhances light absorption.

(A) Schematic illustration of inverted OPV construction with dual plasmonic structures, and the chemical structures of PBDTTT-C-T and PC<sub>71</sub>BM are shown in the left (reprint with permission Ref. [119]; Copyright 2012 Wiley-VCH Verlag GmbH & Co. KGaA, Weinheim). (B) SEM image of multiple-patterned electrodes containing various nanopost and corrugated grating patterns, and *J*-*V* characteristics of OPVs with and without multiple patterns (reprint with permission Ref. [145]; Copyright 2016 Wiley-VCH Verlag GmbH & Co. KGaA, Weinheim).

to achieve broadband light absorption enhancement. The dual plasmonic nanostructures consisted of a periodic nanograting electrode as the back reflector and metal NPs embedded in the active layer based on PBDTTT-C-T:PC<sub>71</sub>BM. The metallic nanograting increased the interface area and realized a higher FF. Owing to the collective excitation of SPPs, LSPR and their hybridizations, the inverted OPVs with dual plasmonic nanostructures show 8.79% enhancement in PCE, with FF increasing from 58.4% to 62.9% and  $J_{sc}$  improving from 17.07 to 18.39 mA/cm<sup>2</sup>. It was the first report to combine metal NPs with nanograting to extend the enhanced absorption region and improve the PCE, FF and  $J_{sc}$  of OPVs by dual plasmonic effects. LSPR resonance has a hard relationship with the refractive index of the surrounding materials and can be tuned by changing the embedded location in the devices [146]. In order to further improve the performance and reproducibility of OPVs based on the dual plasmonic effects, Choy et al. [147] have optimized the construction of dual plasmonic OPVs: they chose the period of the Ag nanograting anode to be 600 nm, embedded the Au NPs in the electron transport layer instead of the active layer and adopted ZnO as the electron transport material. The optimized devices realized a total visible light trapping ranging from 350 to 800 nm and reached a maximum PCE of 9.62% with excellent reproducibility arising from the dual plasmonic effects, demonstrating the significance of the precise design of the nanostructures and device constructions for high-performance devices.

Recently, Sang Kyu Kwak and Joon Hak Oh et al. reported a multiple-patterned plasmonic nanostructure fabricated by synergistically combining a block co-polymer lithography with NIL technology [145]. The multiple-patterned plasmonic nanostructures contained various nanopost and corrugated grating patterns as shown in Figure 9B. In the multiple-patterned OPVs, multiple plasmon effects were excited via the LSPR and SPP modes. The multiple-patterned electrode also scattered light into the active layer to increase the optical path length. The theoretical simulation and scanning near-field optical microscopy have been performed to substantiate the strong multiple plasmonic effects of the multiple-patterned plasmonic electrodes in boosting device performance.

### 3.3 Optical cavity manipulates light

For a planar thin-film OPVs, light trapping strongly depends on the sandwiched device structure with a transparent or semitransparent front electrode and a reflective back electrode. In order to trap photons in the photoactive

region of planar devices, various strategies have been explored, and the most directive approach is to construct an optical cavity configuration to realize optical trapping inside OPVs [148–151]. In this section, three strategies for effective light trapping in OPVs will be discussed and elucidated.

#### 3.3.1 Metal-mirror resonant microcavity

A metal-mirror resonant microcavity is formed when an organic active layer is sandwiched by two reflective metal electrodes. Incident light with resonant frequencies can be trapped inside the metal microcavity, satisfying the constructive interference condition, which realizes the effective light trapping in the sandwiched active layer [152–154]. Ultrathin metal films are usually chosen as the semitransparent front electrode with superior reflective transparent characteristics compared with the commonly used transparent ITO electrode, which ensures the formation of a stronger microcavity to enhance the optical confinement in OPVs. In order to suppress the Volmer-Weber growth mode of the deposited ultrathin metal film and to improve the optical and electronic characteristics of the ultrathin electrode, nucleation-inducing seed layers are commonly required, such as metal seeds, metal oxides and organic materials [35, 155–157]. The nucleation-inducing seed layers can also act as the capping layer or charge transforming layer in OPVs to verify the reflective transparent properties or charge collective properties in bottom-illuminated or top-illuminated OPVs, respectively [158–160].

Jen et al. [152, 161, 162] have demonstrated ITO-free OPVs with the microcavity structure based on an ultrathin Ag electrode. The transmitted incident light through the ultrathin Ag electrode resonated within the optical microcavity, and photons with resonant frequencies were trapped owing to the coherent interference. Figure 10A illustrated the improved exciton generation rate of the microcavity-based devices compared with the ITO-based devices, which was beneficial for the enhanced light absorption by the metal resonant microcavity as well as the improved conversion efficiency of the trapped photons by the ultrathin Ag electrode.

#### 3.3.2 Optical spacer

In typical planar OPVs, the incident light passing through the transparent front electrode is absorbed firstly by the photoactive layers, and the unabsorbed light is then reflected by the metal back electrode. Owing to the optical

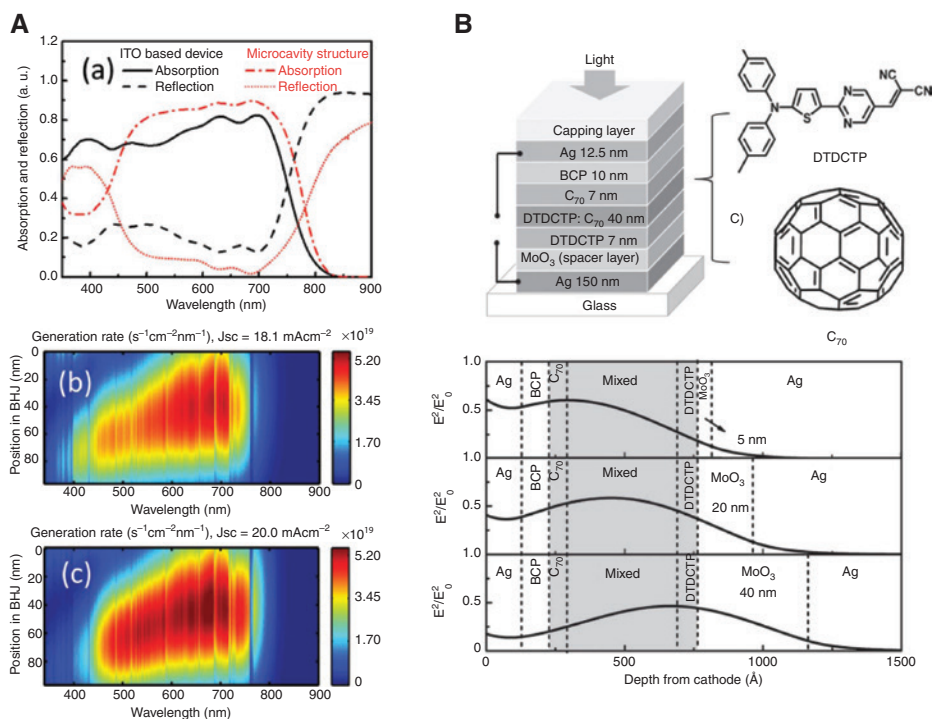


**Figure 10:** Microcavity-based OPVs and Optical-spacer-based OPVs.

(A) Absorption and reflection curves of ITO-based OPVs and microcavity-based OPVs (up), simulated exciton generation profile for ITO-based OPVs (middle) and microcavity-based OPVs (bottom) (reprint with permission Ref. [161]; Copyright 2015 WILEY-VCH Verlag GmbH & Co. KGaA, Weinheim). (B) Device structure and molecular structures of active layer materials, and calculated optical-field distributions at the wavelength of 590 nm. The gray areas are the active layers (reprint with permission Ref. [163]; Copyright 2012 Wiley-VCH Verlag GmbH & Co. KGaA, Weinheim).

interference between the back-reflected light and the incident light, a standing wave with strong oscillation of the optical field within the multilayer structure of the OPVs is generated. The intensity of the optical field is nearly zero at the interface of the reflective metal back electrode. Photoactive materials near the dead zone have minimal contribution to the overall light absorption with significantly reduced photo-generated carriers because of the weak optical field. Constructing an optical spacer is an effective approach to spatially redistribute the optical field inside OPVs [164–166]. The additional optical spacer can alter the optical interference in the multilayer OPVs to modulate the intensity of light in the photoactive layer, and an improved exciton generation can be expected because of the enhanced light harvesting [112]. The work function and charge transmission performance of the inserted optical spacer inside the OPVs should also be taken into consideration, which are key influencing factors for the performance of OPVs, and the inserted optical spacer commonly acts as the charge transmission or extraction layer. Forrest et al. [167] incorporated an organic layer inside OPVs acting as the optical spacer, and they deposited a bathocuproine (BCP) between the photoactive region and the cathode. The pristine function of the incorporated BCP layer was

exciton blocking in nature to prevent exciton diffusion to the cathode interface and subsequent quenching. Owing to the modified optical field by the exciton blocking layer, the light intensity at the donor-acceptor interface was increased, which led to an increase in efficiency. Lee et al. [168] used a solution-based titanium oxide ( $\text{TiO}_x$ ) layer as the optical spacer in polymer photovoltaic cells, and the PCE was enhanced by approximately 50% compared with the reference sample without the optical spacer.

The thickness of an optical spacer is a key parameter to determine the distribution of optical interference inside the active layer. The optical field distributions with different thickness for the in-cell spacer layer ( $\text{MoO}_3$ ) inside OPVs have been modeled as shown in Figure 10B [163]. The optical field maximum was located at the photoactive layer through tuning the thickness of the in-cell spacer layer. With the optimized thickness of  $\text{MoO}_3$ , photon harvesting was enhanced in the very thin active layer.

### 3.3.3 Optical Tamm states

Recently, a simple, planar multilayer structure has been proposed for the creation of surface waves within the light

cone. It has been shown that such states can be formed at the interface between a photonic crystal (PC) and a metal or a dielectric material. These states have been described as optical Tamm states in analogy with electron states predicted by Tamm that can occur in the energy band gap at a crystal surface. Optical Tamm states exhibit local maximum field intensity at the metal/PC interface. The field intensity decays into the PC due to the Bragg forbidden band effect. Conventional surface plasmons have a wave vector exceeding that of light in vacuum and therefore cannot be directly excited by light that is simply incident on the surface. Optical Tamm states have a zero in-plane wave vector and can be produced by direct optical excitation. Different from the SPP modes with TM polarization, optical Tamm states can be formed in both the TE and TM polarizations [169–171]. So, optical Tamm states exhibit a promising approach in OPVs for light harvesting based on the properties of surface wave as the alternative of SPP excitation without the assistance of nanopatterned structures. Zhang et al. [172] have studied the potential application of optical Tamm states in OPVs and constructed a PC bilayer as the dielectric Bragg mirror with periodically alternating layers of ITO and antimony tin oxide (ATO) as shown in Figure 11. The absorption spectra in the active layer were simulated by FDTD codes, and the Drude model was applied to deal with Ag. Figure 11C shows the simulated overall absorption in the photoactive layer for normal incidence with different numbers of PC bilayers. Compared with the conventional reference OPVs, the broadband photonic harvesting enhancement was realized, and the excitation of the optical Tamm states was demonstrated as well from the field peaking at the Ag/PC interface and exhibiting an oscillating-damping profile into the PC. Owing to the excitation of the broadband optical Tamm states, 35% theoretical absorption enhancement has been obtained with two bilayers including 64-nm ITO and 94-nm ATO. Further theoretical simulation confirmed that the overall enhancement was attributed to the abnormal refractive index variation of the active layer and could be improved by increasing the refractive index contrast of the PC bilayers [173].

Tang et al. [174] verified the significantly enhanced light harvesting and photocurrent in OPVs by the optical Tamm states experimentally. They constructed a semi-transparent inverted OPVs with a high reflector structure including six pairs of  $\text{MoO}_3$  (60 nm)/LiF (90 nm). With the optimizing reflector structure, light trapping was improved at the wavelength region between 450 and 600 nm owing to the effect of the optical Tamm states, and the  $J_{sc}$  was increased from 8.09 to 10.9  $\text{mA}/\text{cm}^2$ , which resulted in a 30% enhancement in PCE compared with the control devices.

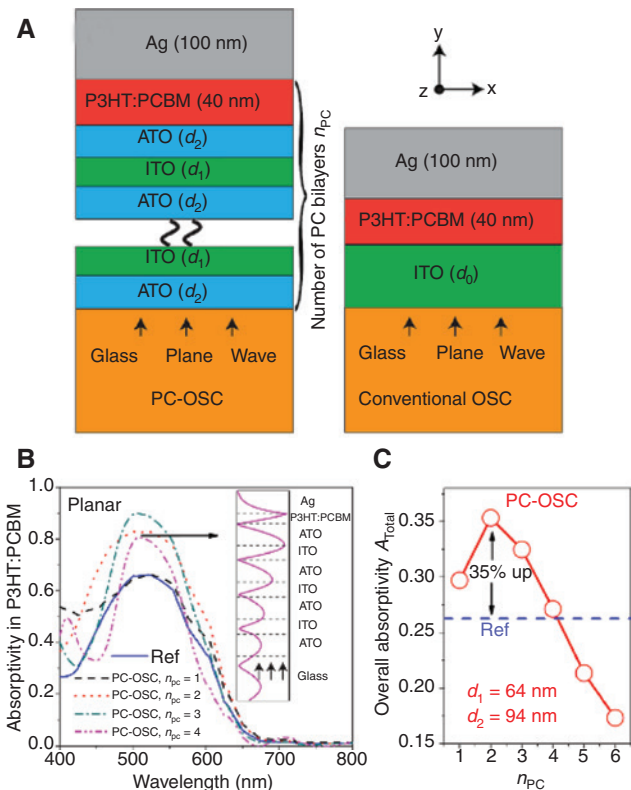


**Figure 11:** Optical Tamm states improve light absorption in OPVs. (A) Device structure of OPVs with designed PC (left) and conventional OPVs (right). (B) Theoretically simulated absorption spectra in the active layer under normal TM-polarized incidence with different numbers of PC bilayers ( $n_{pc}$ ). The active layer was P3HT:PCBM, and the lattice parameters were chosen as  $d_1 = 64$  nm (the thickness of ITO) and  $d_2 = 94$  nm (the thickness of ATO). (C) Simulated overall absorptivity  $A_{Total}$  as a function of  $n_{pc}$  (reprint with permission Ref. [172]; Copyright 2012 American Institute of Physics).

### 3.4 Optical mode cross-coupling in OPVs

Tandem OPVs with two or more stacked single cells is a new candidate for high-performance solar cells with increased open-circuit voltage and PCE [175, 176]. However, because of the nonuniform distribution of incident light in the stacked sub-cells, the photocurrents generated in the different sub-cells are unbalanced, which degenerate the efficiency of the tandem devices. Carefully designing the structure and properly choosing active layers with nonoverlapping absorption wavelength region can overcome this obstacle in tandem OPVs [177, 178]. Feng et al. [179] presented a neoteric solution by introducing a periodical corrugated metal cathode to enhance the light absorption of the back sub-cell in the small molecule-based double-junction tandem OPVs as shown in Figure 12A. In the simulated distribution of the magnetic field intensity of the corrugated tandem OPVs based on a 300-nm period

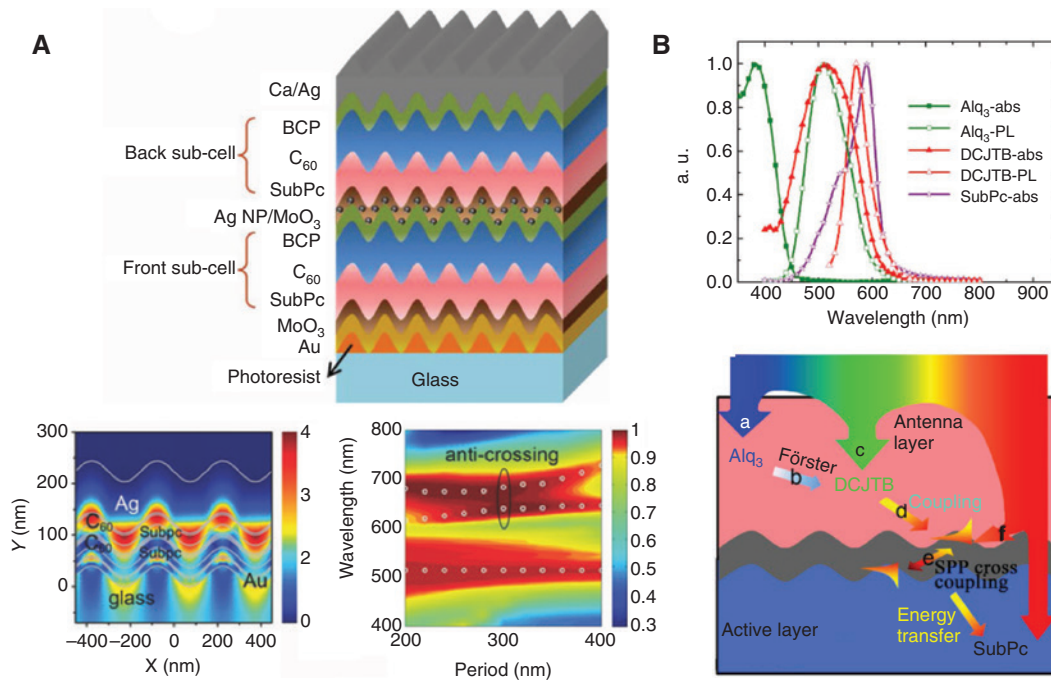


**Figure 12:** Optical mode cross-coupling in OPVs.

(A) Device structure (up), simulated distribution of the magnetic field intensity (left bottom) and dispersion relationship (right bottom) of the corrugated microcavity tandem OPVs (reprint with permission Ref. [179]; Copyright 2013 Wiley-VCH Verlag GmbH and Co. KGaA, Weinheim). (B) The absorption and the PL spectra of the antenna material and the donor material boron subphthalocyanine chloride (SubPc) (up), and the energy transfer mechanism in the corrugated antenna-based OPVs (bottom) (reprint with permission Ref. [180]; Copyright 2015 AIP Publishing LLC).

at 650-nm wavelength, SPP resonance at the interface of the Ag cathode and the back sub-cell can be demonstrated. Meanwhile, the microcavity modes also exist at the interface. From the simulated dispersion relationship of the corrugated devices, an anti-crossing between the SPP mode and the microcavity mode occurs when the period is around 300 nm. This anti-crossing is caused by a strong interference between the SPPs and the microcavity modes at the interface between the Ag cathode and the back sub-cell. The anti-crossing between the SPPs and the microcavity modes has obtained a strong field enhancement in the metal-dielectric-metal structure. Moreover, it leads to a broadband resonance at around 600 nm due to the formation of a large anti-crossing gap. Both theoretical and experimental results supported the anti-crossing of optical modes in devices with enhanced light-trapping behavior. Consequently, the photocurrent and PCE of the double-junction tandem devices with corrugated metal electrode were improved by 10.4% and 11.3%, respectively.

Jin et al. [180] explored another strategy of optical mode cross-coupling in OPVs, and a broadband absorption enhancement was realized in top-incident inverted OPVs with an additional antenna layer on top of the

microstructured metal anode as shown in Figure 12B. The antenna layer consisted of tris-(8-hydroxyquinoline) aluminum (Alq<sub>3</sub>) doped with 1 wt% (4-(dicyanomethylene)-2-*t*-butyl-6-(1,1,7,7-tetramethyljuloli-dyl)-4*H*-pyran (DCJTb). The sufficient overlap spectra between the PL of the donor Alq<sub>3</sub> and the absorption of the acceptor of the DCJTb result in an efficient Förster energy transfer from Alq<sub>3</sub> to DCJTb. The energy transfer from the DCJTb to the photoactive materials is also reliable due to the sufficient overlap between the PL spectra of the DCJTb and the absorption spectra of SubPc. The corrugated metal electrode has been employed to excite SPP resonance to transfer molecular excitation energy from DCJTb to SubPc, crossing the thick metallic electrode. As a consequence, the trapped energy by the antenna material was coupled and transferred to the active layer by cross-coupling of the SPP modes at the interface of the Ag anode and the antenna layer. Owing to the complementary absorption property of the antenna layer compared with the active layer in OPVs, a broadband-enhanced light absorption has been realized. Compared with the planar reference sample, the corrugated OPVs based on the antenna layer obtained a 16% improvement in PCE, with the  $J_{sc}$  increased from 6.07 to 6.98 mA/cm<sup>2</sup>.

## 4 Conclusions and outlook

In this review, we have discussed the optical engineering in OPVs to improve light absorption in thin photoactive layers. Owing to the tradeoff between the efficiency of photon absorption and exciton harvesting, the thickness of the photoactive layer is limited, which results in incomplete light absorption. We reviewed light-trapping strategies by incorporating nanostructures or nanomaterials outside and inside the active layers in OPVs, as well as the fabrication technologies for the nanostructures or nanomaterials. By introducing out-of-cell nanostructures on the transparent substrates and electrodes, the reflective losses of incident light are suppressed. However, the antireflective geometries suffer from the complex and uneconomical fabrication processes, especially the lack of compatibility with roll-to-roll technologies for large-area fabrication. Plasmonic nanostructures and nanomaterials engaged inside cells, such as periodic grating, metal NPs and freedom corrugation, couple the incident photons in the photoactive layers by the simplex or collective effects of plasmonic scattering, SPPs and LSPR. Unfortunately, the resonant wavelength of metal nanomaterials is typically narrow, determined by the nanomaterials size, shape and their surrounding materials. The quenching of excited states in the interface of plasmonic nanostructures decreases the improvement of the performance of OPVs. In addition, the polarization dependence and angle sensitivity of SPPs pose a limitation for OPV applications. Consequently, it is still critical to design the plasmonic

nanomaterials and nanostructures with broadband, polarization-independent and angle-insensitive light trapping. Furthermore, parasitic absorption in plasmonic electrodes is omnipresent and must be considered alongside the potential optical benefits of plasmonic electrodes for OPV applications. Tailoring the optical field distribution by designing optical cavities in OPVs to manipulate light also enables the light absorption to reach high value in thin active layers. The engaged optical spacer and PC bilayers with a precise control of lattice thicknesses result in more complicated fabrication processes than the fabrication of nanopatterned structures, and the electrical properties of the inset layers also affect the efficiency of OPVs. The improved OPVs based on various light-manipulating approaches are listed in Table 2. It is not apparent that a particular light-trapping strategy is substantially better for OPV applications than the others. Depending on the device architecture, the active layer material properties and the location in the device stack, it is clear that certain or complex approaches will play a more important role in enhancing the efficiency of devices, which should be assessed on a case-by-case basis.

Benefitting from the progress made in material development and device optimization, OPVs have demonstrated remarkable improvement in the past few years. So far, the light-manipulating strategies for photon harvesting mostly focused on devices with small size, and it will be interesting to construct and fabricate solution-processed microstructured OPVs with large scale and low cost, especially based on the roll-to-roll technology. In addition,

**Table 2:** The improved performance of OPVs by the nanopattern-induced light trapping.

Donor:Acceptor	Geometry	PCE (%)	PCEref (%)	EF (%)	Mechanisms	Ref.
PDPPT:PCBM	Texture sheet	5.5	4.6	19	Antireflection, increase light path	[81]
SubPc:C <sub>60</sub>	Microlens array	3.7	3.1	19	Antireflection, increase light path	[86]
CuPc:C <sub>60</sub>	Ag grating	1.07	1.44	35	SPP	[10]
P3HT:PCBM	1-D grating	4.1	3.6	14	SPP	[114]
	2-D grating	4.3	3.6	19		
SubPc:C <sub>60</sub>	Dual period grating	3.5	2.6	31	Broadband SPP	[44]
P3HT:ICBA	Biomimetic moth's eye antireflective layer	7.8	6.4	22	SPP, light scattering, antireflection	[99]
P3HT:PCBM	Ag NPs and nanoprisms	4.3	3.6	18	Broadband LSPR	[92]
P3HT:PCBM	Ag@oxide nanoprisms	4.0	3.1	31	LSPR	[130]
PCDTBT:PCBM	Ag NPs in MoO <sub>3</sub>	5.8	5.07	14	LSPR	[137]
PTB7:PCBM	Au@Ag NPs	9.2	7.9	16	LSPR	[110]
P3HT:PCBM	Au NPs and Ag grating	4.06	3.07	30	LSPR and SPP	[147]
PBDTTT-C-T:PCBM	Multiple patterns	9.63	7.75	24	SPP, light scattering	[145]
P3HT:PCBM	TiOx insert Layer	12.6	8.1	50	Optical spacer	[168]
P3HT:PCBM	6 MoO <sub>3</sub> /LiF layers	4.32	3.36	29	Optical Tamm states	[174]
SubPc:C <sub>60</sub>	Ag grating, metal electrode, Ag NPs	6.10	5.48	11	Coupling of SPP and microcavity, LSPR	[179]
SubPc:C <sub>60</sub>	Ag grating and an antenna layer	3.89	3.35	16	Cross-coupling of SPP and antenna	[180]

PCEref, the PCE of reference sample; EF, enhancement factor.

except for efficiency, stability and lifetime are also the key factors that should be considered and researched for the commercial application of OPVs. Therefore, understanding the potential influence of the nanostructures on the stability and lifetime of OPVs requires stringent fundamental research. We summarized here the state-of-the-art light manipulation technologies in OPVs in the hope to drive the application of OPVs with high efficiency, long lifetime and stability.

**Acknowledgments:** This work was supported by National Natural Science Foundation of China (NSFC) under Grants #61705075, #61675085, #61590930, #61435005, and #51335008, National Key Research and Development Program of China (Grant No. 2017YFB0404501) and China Postdoctoral Science Foundation (Grant No. 2016M600230).

## References

- [1] Brabec CJ, Gowrisanker S, Halls JMM, Laird D, Jia SJ, Williams SP. Polymer-fullerene bulk-heterojunction solar cells. *Adv Mater* 2010;22:3839–56.
- [2] Hau SK, Yip HL, Jen AKY. A review on the development of the inverted polymer solar cell architecture. *Polym Rev* 2010;50:474–510.
- [3] Zheng Y, Xue JG. Organic photovoltaic cells based on molecular donor-acceptor heterojunctions. *Polym Rev* 2010;50:420–53.
- [4] Yan Y, Cai FL, Yang LY, et al. Light-soaking-free inverted polymer solar cells with an efficiency of 10.5% by compositional and surface modifications to a low-temperature-processed TiO<sub>2</sub> electron-transport layer. *Adv Mater* 2017;29:1604044.
- [5] Botiz I, Darling SB. Optoelectronics using block copolymers. *Mater Today* 2010;13:42–51.
- [6] Facchetti A. Polymer donor–polymer acceptor (all-polymer) solar cells. *Mater Today* 2013;16:123–32.
- [7] Darling SB, You FQ. The case for organic photovoltaics. *RSC Adv* 2013;3:17633–48.
- [8] Mazzi KA, Luscombe CK. The future of organic photovoltaics. *Chem Soc Rev* 2015;44:78–90.
- [9] Tang CW. Two-layer organic photovoltaic cell. *Appl Phys Lett* 1986;48:183–5.
- [10] Jin Y, Feng J, Zhang X-L, et al. Surface-plasmon enhanced absorption in organic solar cells by employing a periodically corrugated metallic electrode. *Appl Phys Lett* 2012;101:163303.
- [11] Min C, Li J, Veronis G, Lee J-Y, Fan S, Peumans P. Enhancement of optical absorption in thin-film organic solar cells through the excitation of plasmonic modes in metallic gratings. *Appl Phys Lett* 2010;96:133302.
- [12] Xu W-F, Chin C-C, Hung D-W, Wei P-K. Transparent electrode for organic solar cells using multilayer structures with nanoporous silver film. *Sol Energy Mater Sol Cells* 2013;118:81–9.
- [13] Zeng W, Yong KS, Kam ZM, Zhu F, Li Y. Effect of blend layer morphology on performance of ZnPc:C60-based photovoltaic cells. *Appl Phys Lett* 2010;97:133304.
- [14] Kim K, Carroll DL. Roles of Au and Ag nanoparticles in efficiency enhancement of poly(3-octylthiophene)/C60 bulk heterojunction photovoltaic devices. *Appl Phys Lett* 2005;87:203113.
- [15] Su ZS, Wang LD, Li YT, et al. Surface plasmon enhanced organic solar cells with a MoO<sub>3</sub> buffer layer. *ACS Appl Mater Interfaces* 2013;5:12847–53.
- [16] Li G, Shrotriya V, Huang JS, et al. High-efficiency solution processable polymer photovoltaic cells by self-organization of polymer blends. *Nat Mater* 2005;4:864–8.
- [17] Niesen B, Rand BP, Van Dorpe P, et al. Plasmonic efficiency enhancement of high performance organic solar cells with a nanostructured rear electrode. *Adv Energy Mater* 2013;3:145–50.
- [18] Liang Y, Feng D, Wu Y, et al. Highly efficient solar cell polymers developed via fine-tuning of structural and electronic properties. *J Am Chem Soc* 2009;131:7792–9.
- [19] Yu HZ, Peng JB. Performance and lifetime improvement of polymer/fullerene blend photovoltaic cells with a C60 interlayer. *Org Electron* 2008;9:1022–5.
- [20] Liang YY, Xu Z, Xia JB, et al. For the bright future-bulk heterojunction polymer solar cells with power conversion efficiency of 7.4%. *Adv Energy Mater* 2010;22:E135–8.
- [21] Huo L, Zhang S, Guo X, Xu F, Li Y, Hou J. Replacing alkoxy groups with alkylthienyl groups: a feasible approach to improve the properties of photovoltaic polymers. *Angew Chem Int Ed* 2011;50:9697–702.
- [22] Li X, Choy WCH, Huo L, et al. Dual plasmonic nanostructures for high performance inverted organic solar cells. *Adv Mater* 2012;24:3046–52.
- [23] You JB, Chen CC, Dou LT, et al. Metal oxide nanoparticles as an electron-transport layer in high-performance and stable inverted polymer solar cells. *Adv Mater* 2012;24:5267–72.
- [24] Wen XM, Ma R, Yin D, Bi YG. Efficient inverted flexible polymer solar cells with transparent top MoO<sub>3</sub>/Au/Ag/NPB electrodes. *Opt Mater Express* 2017;7:2188–93.
- [25] Wang CCD, Choy WCH, Duan C, et al. Optical and electrical effects of gold nanoparticles in the active layer of polymer solar cells. *J Mater Chem* 2012;22:1206–11.
- [26] Walker B, Tomayo AB, Dang XD, et al. Nanoscale phase separation and high photovoltaic efficiency in solution-processed, small-molecule bulk heterojunction solar cells. *Adv Funct Mater* 2009;19:3063–9.
- [27] Sun YM, Welch GC, Leong WL, Takacs CJ, Bazan GC, Heeger AJ. Solution-processed small-molecule solar cells with 6.7% efficiency. *Nat Mater* 2012;11:44–8.
- [28] Ahn S, Rourke D, Park W. Plasmonic nanostructures for organic photovoltaic devices. *J Opt* 2016;18:033001.
- [29] Lim EL, Yap CC, Teridi MAM, Teh CH, Yusoff ARBM, Jumali MHH. A review of recent plasmonic nanoparticles incorporated P3HT:PCBM organic thin film solar cells. *Org Electron* 2016;36:12–28.
- [30] Zhou N, Lopez-Puente V, Wang Q, Polavarapu L, Pastoriza-Santos I, Xu Q-H. Plasmon-enhanced light harvesting: applications in enhanced photocatalysis, photodynamic therapy and photovoltaics. *RSC Adv* 2015;5:29076–97.
- [31] Haugeneder A, Neges M, Kallinger C, et al. Exciton diffusion and dissociation in conjugated polymer fullerene blends and heterostructures. *Phys Rev B* 1999;59:15346–51.
- [32] Li WW, Hendriks KH, Roelofs WSC, Kim Y, Wienk MM, Janssen RAJ. Efficient small bandgap polymer solar cells with high fill factors for 300 nm thick films. *Adv Mater* 2013;25:3182–6.

- [33] Li WT, Abrecht S, Yang LQ, et al. Mobility-controlled performance of thick solar cells based on fluorinated copolymers. *J Am Chem Soc* 2014;136:15566–76.
- [34] Duche D, Drouard E, Simon JJ, et al. Light harvesting in organic solar cells. *Sol Energy Mater Sol Cells* 2011;95:S18–25.
- [35] Han YC, Lim MS, Park JH, Choi KC. ITO-free flexible organic light-emitting diode using ZnS/Ag/MoO<sub>3</sub> anode incorporating a quasi-perfect Ag thin film. *Org Electron* 2013;14:3437–43.
- [36] Ko SJ, Choi H, Lee W, et al. Highly efficient plasmonic organic optoelectronic devices based on a conducting polymer electrode incorporated with silver nanoparticles. *Energy Environ Sci* 2013;6:1949–55.
- [37] Atwater HA, Polman A. Plasmonics for improved photovoltaic devices. *Nat Mater* 2010;9:205–13.
- [38] Guo CF, Sun TY, Cao F, Liu Q, Ren ZF. Metallic nanostructures for light trapping in energy-harvesting devices. *Light-Sci Appl* 2014;3:e161.
- [39] Zhang X-L, Song J-F, Li X-B, Feng J, Sun H-B. Anti-reflection resonance in distributed Bragg reflectors-based ultrathin highly absorbing dielectric and its application in solar cells. *Appl Phys Lett* 2013;102:103901.
- [40] Gilot J, Barbu I, Wienk MM, Janssen RAJ. The use of ZnO as optical spacer in polymer solar cells: theoretical and experimental study. *Appl Phys Lett* 2007;91:113520.
- [41] Zhang Y-L, Chen Q-D, Xia H, Sun H-B. Designable 3D nanofabrication by femtosecond laser direct writing. *Nano Today* 2010;5:435–48.
- [42] Sugioka K, Cheng Y. Femtosecond laser processing for optofluidic fabrication. *Lab Chip* 2012;12:3576–89.
- [43] Fang RR, Vorobyev A, Guo CL. Direct visualization of the complete evolution of femtosecond laser-induced surface structural dynamics of metals. *Light-Sci Appl* 2017;6:e16256.
- [44] Bi Y-G, Feng J, Chen Y, et al. Dual-periodic-corrugation-induced broadband light absorption enhancement in organic solar cells. *Org Electron* 2015;27:167–72.
- [45] Bai Y, Feng J, Liu Y-F, et al. Outcoupling of trapped optical modes in organic light-emitting devices with one-step fabricated periodic corrugation by laser ablation. *Org Electron* 2011;12:1927–35.
- [46] Bi Y-G, Feng J, Li Y-F, et al. Broadband light extraction from white organic light-emitting devices by employing corrugated metallic electrodes with dual periodicity. *Adv Mater* 2013;25:6969–74.
- [47] Abid MI, Wang L, Chen Q-D, Wang X-W, Juodkakis S, Sun H-B. Angle-multiplexed optical printing of biomimetic hierarchical 3D textures. *Laser Photon Rev* 2017;11:1600187.
- [48] Wu D, Wu S-Z, Zhao S, et al. Rapid, controllable fabrication of regular complex microarchitectures by capillary assembly of micropillars and their application in selectively trapping/releasing microparticles. *Small* 2013;9:760–7.
- [49] Schiff H. Nanoimprint lithography: 2D or not 2D? A review. *Appl Phys A-Mater Sci Process* 2015;121:415–35.
- [50] Khang DY, Yoon H, Lee HH. Room-temperature imprint lithography. *Adv Mater* 2001;13:749–52.
- [51] Chou SY, Krauss PR, Renstrom PJ. Imprint of sub-25 nm vias and trenches in polymers. *Appl Phys Lett* 1995;67:3114–6.
- [52] Chou SY, Krauss PR, Zhang W, Guo L, Zhuang L. Sub-10 nm imprint lithography and applications. *J Vac Sci Technol B: Microelectron Nanometer Struct Proces Meas Phenom* 1997;15:2897–904.
- [53] Malaquin L, Carcenac F, Vieu C, Mauzac M. Using polydimethylsiloxane as a thermocurable resist for a soft imprint lithography process. *Microelectron Eng* 2002;61–62:379–84.
- [54] Chen YF. Applications of nanoimprint lithography/hot embossing: a review. *Appl Phys A-Mater Sci Process* 2015;121:451–65.
- [55] Schiff H. Nanoimprint lithography: an old story in modern times? A review. *J Vac Sci Technol B: Microelectron Nanometer Struct Proces Meas Phenom* 2008;26:458–80.
- [56] Haisma J, Verheijen M, Heuvel KVD, Berg JVD. Mold-assisted nanolithography: a process for reliable pattern replication. *J Vac Sci Technol B: Microelectron Nanometer Struct Proces Meas Phenom* 1996;14:4124–8.
- [57] Wen-chang L, Steve Lien-Chung H. A novel liquid thermal polymerization resist for nanoimprint lithography with low shrinkage and high flowability. *Nanotechnology* 2007;18:065303.
- [58] Kang MG, Kim MS, Kim JS, Guo LJ. Organic solar cells using nanoimprinted transparent metal electrodes. *Adv Mater* 2008;20:4408–13.
- [59] Gröning P, Schneuwly A, Schlapbach L, Gale MT. “Self-thickness-limited” plasma polymerization of an ultrathin antiadhesive film. *J Vac Sci Technol A* 1996;14:3043–8.
- [60] Yoshikawa H, Taniguchi J, Tazaki G, Zento T. Fabrication of high-aspect-ratio pattern via high throughput roll-to-roll ultraviolet nanoimprint lithography. *Microelectron Eng* 2013;112:273–7.
- [61] Ahn SH, Guo LJ. High-speed roll-to-roll nanoimprint lithography on flexible plastic substrates. *Adv Mater* 2008;20:2044–9.
- [62] Koo WH, Jeong SM, Araoka F, et al. Light extraction from organic light-emitting diodes enhanced by spontaneously formed buckles. *Nat Photonics* 2010;4:222–6.
- [63] Okayasu T, Zhang HL, Bucknall DG, Briggs GAD. Spontaneous formation of ordered lateral patterns in polymer thin-film structures. *Adv Funct Mater* 2004;14:1081–8.
- [64] Koo WH, Jeong SM, Nishimura S, et al. Polarization conversion in surface-plasmon-coupled emission from organic light-emitting diodes using spontaneously formed buckles. *Adv Mater* 2011;23:1003–7.
- [65] Stafford CM, Harrison C, Beers KL, et al. A buckling-based metrology for measuring the elastic moduli of polymeric thin films. *Nat Mater* 2004;3:545–50.
- [66] Sun Y, Kumar V, Adesida I, Rogers JA. Buckled and wavy ribbons of GaAs for high-performance electronics on elastomeric substrates. *Adv Mater* 2006;18:2857–62.
- [67] Khang D-Y, Jiang H, Huang Y, Rogers JA. A stretchable form of single-crystal silicon for high-performance electronics on rubber substrates. *Science* 2006;311:208–12.
- [68] Bowden N, Brittain S, Evans AG, Hutchinson JW, Whitesides GM. Spontaneous formation of ordered structures in thin films of metals supported on an elastomeric polymer. *Nature* 1998;393:146–9.
- [69] Li SP, Chu DP, Koltsov DK, Fu YT, Welland ME. Spontaneous formation of highly ordered nanostructures: thermal instability and mode selection in surface-capped polymer films. *Nanotechnology* 2008;19:235302.
- [70] Bowden N, Huck WTS, Paul KE, Whitesides GM. The controlled formation of ordered, sinusoidal structures by plasma oxidation of an elastomeric polymer. *Appl Phys Lett* 1999;75:2557–9.
- [71] Huck WTS, Bowden N, Onck P, Pardoen T, Hutchinson JW, Whitesides GM. Ordering of spontaneously formed buckles on planar surfaces. *Langmuir* 2000;16:3497–501.

- [72] Chen X, Jia B, Zhang Y, Gu M. Exceeding the limit of plasmonic light trapping in textured screen-printed solar cells using Al nanoparticles and wrinkle-like graphene sheets. *Light Sci Appl* 2013;2:e92.
- [73] Murray WA, Barnes WL. Plasmonic materials. *Adv Mater* 2007;19:3771–82.
- [74] Lee J-S, Cho J, Lee C, et al. Layer-by-layer assembled charge-trap memory devices with adjustable electronic properties. *Nat Nanotechnol* 2007;2:790–5.
- [75] Xu M, Feng J, Liu Y-S, Jin Y, Wang H-Y, Sun H-B. Effective and tunable light trapping in bulk heterojunction organic solar cells by employing Au-Ag alloy nanoparticles. *Appl Phys Lett* 2014;105:153303.
- [76] Mallik K, Mandal M, Pradhan N, Pal T. Seed mediated formation of bimetallic nanoparticles by UV irradiation: a photochemical approach for the preparation of “core-shell” type structures. *Nano Lett* 2001;1:319–22.
- [77] Qingbo Z, Jim Yang L, Jun Y, Chris B, Jixuan Z. Size and composition tunable Ag–Au alloy nanoparticles by replacement reactions. *Nanotechnology* 2007;18:245605.
- [78] Li ZY, Wilcoxon JP, Yin F, Chen Y, Palmer RE, Johnston RL. Structures and optical properties of 4–5 nm bimetallic AgAu nanoparticles. *Faraday Discuss* 2008;138:363–73.
- [79] Harada M, Asakura K, Toshima N. Catalytic activity and structural analysis of polymer-protected gold/palladium bimetallic clusters prepared by the successive reduction of hydrogen tetrachloroaurate(III) and palladium dichloride. *J Phys Chem* 1993;97:5103–14.
- [80] Kelly KL, Coronado E, Zhao LL, Schatz GC. The optical properties of metal nanoparticles: the influence of size, shape, and dielectric environment. *J Phys Chem B* 2003;107:668–77.
- [81] Esiner S, Bus T, Wienk MM, Hermans K, Janssen RAJ. Quantification and validation of the efficiency enhancement reached by application of a retroreflective light trapping texture on a polymer solar cell. *Adv Energy Mater* 2013;3:1013–7.
- [82] Tvingstedt K, Zilio SD, Inganäs O, Tormen M. Trapping light with micro lenses in thin film organic photovoltaic cells. *Opt Express* 2008;16:21608–15.
- [83] Luhman WA, Lee SH, Johnson TW, Holmes RJ, Oh S-H. Self-assembled plasmonic electrodes for high-performance organic photovoltaic cells. *Appl Phys Lett* 2011;99:103306.
- [84] Lampande R, Kim GW, Park MJ, Kang BY, Kwon JH. Efficient light harvesting in inverted polymer solar cells using polymeric 2D-microstructures. *Sol Energy Mater Sol Cells* 2016;151:162–8.
- [85] Huang Z-Y, Chiu S-W, Chen C-W, et al. Spontaneous formation of light-trapping nano-structures for top-illumination organic solar cells. *Nanoscale* 2014;6:2316–20.
- [86] Myers JD, Cao W, Cassidy V, et al. A universal optical approach to enhancing efficiency of organic-based photovoltaic devices. *Energy Environ Sci* 2012;5:6900–4.
- [87] Hiralal P, Chien C, Lal NN, et al. Nanowire-based multifunctional antireflection coatings for solar cells. *Nanoscale* 2014;6:14555–62.
- [88] Baba A, Aoki N, Shinbo K, Kato K, Kaneko F. Grating-coupled surface plasmon enhanced short-circuit current in organic thin-film photovoltaic cells. *ACS Appl Mater Interfaces* 2011;3:2080–4.
- [89] Khan I, Keshmiri H, Kolb F, Dimopoulos T, List-Kratochvil EJW, Dostalek J. Multidiffractive broadband plasmonic absorber. *Adv Opt Mater* 2016;4:435–43.
- [90] Tumbleston JR, Gadisa A, Liu Y, et al. Modifications in morphology resulting from nanoimprinting bulk heterojunction blends for light trapping organic solar cell designs. *ACS Appl Mater Interfaces* 2013;5:8225–30.
- [91] Chen MC, Yang YL, Chen SW, Li JH, Aklilu M, Tai Y. Self-assembled monolayer immobilized gold nanoparticles for plasmonic effects in small molecule organic photovoltaic. *ACS Appl Mater Interfaces* 2013;5:511–7.
- [92] Li X, Choy WCH, Lu H, Sha WEI, Ho AHP. Efficiency enhancement of organic solar cells by using shape-dependent broadband plasmonic absorption in metallic nanoparticles. *Adv Funct Mater* 2013;23:2728–35.
- [93] Shahin S, Gangopadhyay P, Norwood RA. Ultrathin organic bulk heterojunction solar cells: plasmon enhanced performance using Au nanoparticles. *Appl Phys Lett* 2012;101:053109.
- [94] Noh HS, Cho EH, Kim HM, Han YD, Joo J. Organic solar cells using plasmonics of Ag nanoprisms. *Org Electron* 2013;14:278–85.
- [95] Reilly TH, van de Lagemaat J, Tenent RC, Morfa AJ, Rowlen KL. Surface-plasmon enhanced transparent electrodes in organic photovoltaics. *Appl Phys Lett* 2008;92:243304.
- [96] Ostfeld AE, Pacifici D. Plasmonic concentrators for enhanced light absorption in ultrathin film organic photovoltaics. *Appl Phys Lett* 2011;98:243304.
- [97] Li X, Hu Y, Deng Z, et al. Efficiency improvement of polymer solar cells with random micro-nanostructured back electrode formed by active layer self-aggregation. *Org Electron* 2017;41:362–8.
- [98] Leem JW, Kim S, Park C, Kim E, Yu JS. Strong photocurrent enhancements in plasmonic organic photovoltaics by biomimetic nanoarchitectures with efficient light harvesting. *ACS Appl Mater Interfaces* 2015;7:6706–15.
- [99] Chen JD, Zhou L, Ou QD, et al. Enhanced light harvesting in organic solar cells featuring a biomimetic active layer and a self-cleaning antireflective coating. *Adv Energy Mater* 2014;4:1301777.
- [100] Lan W, Cui Y, Yang Q, Lo M-F, Lee C-S, Zhu F. Broadband light absorption enhancement in moth’s eye nanostructured organic solar cells. *Aip Adv* 2015;5:057164.
- [101] Basu Mallick S, Sergeant NP, Agrawal M, Lee J-Y, Peumans P. Coherent light trapping in thin-film photovoltaics. *Mrs Bulletin* 2011;36:453–60.
- [102] Wang X, Deng Y, Li QT, et al. Excitation and propagation of surface plasmon polaritons on a non-structured surface with a permittivity gradient. *Light-Sci Appl* 2016;5:e16179.
- [103] Ozbay E. Plasmonics: merging photonics and electronics at nanoscale dimensions. *Science* 2006;311:189–93.
- [104] Ivinskaya A, Petrov MI, Bogdanov AA, Shishkin I, Ginzburg P, Shalin AS. Plasmon-assisted optical trapping and anti-trapping. *Light-Sci Appl* 2017;6:e16258.
- [105] Zhan Y, Zhao J, Zhou C, Wang X, Li Y, Li Y. Surface-plasma-coupled photovoltaic cell with double-layered triangular grating. *IEEE Photon J* 2012;4:1021–6.
- [106] de Oliveira Hansen RM, Liu Y, Madsen M, Rubahn H-G. Flexible organic solar cells including efficiency enhancing grating structures. *Nanotechnology* 2013;24:145301.
- [107] Lee S, In S, Mason DR, Park N. Incorporation of nanovoids into metallic gratings for broadband plasmonic organic solar cells. *Opt Express* 2013;21:4055–60.

- [108] Kim C, Shtein M, Forrest SR. Nanolithography based on patterned metal transfer and its application to organic electronic devices. *Appl Phys Lett* 2002;80:4051–3.
- [109] Aryal M, Trivedi K, Hu W. Nano-confinement induced chain alignment in ordered p3ht nanostructures defined by nanoimprint lithography. *Acs Nano* 2009;3:3085–90.
- [110] Baek S-W, Park G, Noh J, et al. Au@Ag Core-shell nanocubes for efficient plasmonic light scattering effect in low bandgap organic solar cells. *Acs Nano* 2014;8:3302–12.
- [111] Gan Q, Bartoli FJ, Kafafi ZH. Plasmonic-enhanced organic photovoltaics: breaking the 10% efficiency barrier. *Adv Mater* 2013;25:2385–96.
- [112] Chueh C-C, Crump M, Jen AKY. Optical enhancement via electrode designs for high-performance polymer solar cells. *Adv Funct Mater* 2016;26:321–40.
- [113] Li X, Choy WCH, Ren X, Xin J, Lin P, Leung DCW. Polarization-independent efficiency enhancement of organic solar cells by using 3-dimensional plasmonic electrode. *Appl Phys Lett* 2013;102:153304.
- [114] Na SI, Kim SS, Jo J, Oh SH, Kim J, Kim DY. Efficient polymer solar cells with surface relief gratings fabricated by simple soft lithography. *Adv Funct Mater* 2008;18:3956–63.
- [115] In S, Park N. Inverted ultrathin organic solar cells with a quasi-grating structure for efficient carrier collection and dip-less visible optical absorption. *Sci Rep* 2016;6:21784.
- [116] Chen JD, Cui CH, Li YQ, et al. Single-junction polymer solar cells exceeding 10% power conversion efficiency. *Adv Mater* 2015;27:1035–41.
- [117] Zhou L, Ou Q-D, Chen J-D, et al. Light manipulation for organic optoelectronics using bio-inspired moth's eye nanostructures. *Sci Rep* 2014;4:4040.
- [118] Cho S, Kim KD, Heo J, et al. Role of additional PCBM layer between ZnO and photoactive layers in inverted bulk-heterojunction solar cells. *Sci Rep* 2014;4:4306.
- [119] Li XH, Choy WCH, Huo LJ, et al. Dual plasmonic nanostructures for high performance inverted organic solar cells. *Adv Mater* 2012;24:3046–52.
- [120] Hlaing H, Lu XH, Hofmann T, Yager KG, Black CT, Ocko BM. Nanoimprint-induced molecular orientation in semiconducting polymer nanostructures. *Acs Nano* 2011;5:7532–8.
- [121] Sha WEI, Li XH, Choy WCH. Breaking the space charge limit in organic solar cells by a novel plasmonic-electrical concept. *Sci Rep* 2014;4:6236.
- [122] Yang YG, Feng SL, Li M, et al. Structure, optical absorption, and performance of organic solar cells improved by gold nanoparticles in buffer layers. *ACS Appl Mater Interfaces* 2015;7:24430–37.
- [123] Heo M, Cho H, Jung JW, Jeong JR, Park S, Kim JY. High-performance organic optoelectronic devices enhanced by surface plasmon resonance. *Adv Mater* 2011;23:5689–93.
- [124] Fan G-Q, Zhuo Q-Q, Zhu J-J, et al. Plasmonic-enhanced polymer solar cells incorporating solution-processable Au nanoparticle-adhered graphene oxide. *J Mater Chem* 2012;22:15614–19.
- [125] Karabchevsky A, Mosayyebi A, Kavokin AV. Tuning the chemiluminescence of a luminol flow using plasmonic nanoparticles. *Light-Sci Appl* 2016;5:e16164.
- [126] Liu C, Zhao C, Zhang X, Guo W, Liu K, Ruan S. Unique gold nanorods embedded active layer enabling strong plasmonic effect to improve the performance of polymer photovoltaic devices. *J Phys Chem C* 2016;120:6198–205.
- [127] Topp K, Borchert H, Johnen F, et al. Impact of the incorporation of Au nanoparticles into polymer/fullerene solar cells. *J Phys Chem A* 2010;114:3981–9.
- [128] Xue M, Li L, de Villiers BJT, et al. Charge-carrier dynamics in hybrid plasmonic organic solar cells with Ag nanoparticles. *Appl Phys Lett* 2011;98:253302.
- [129] Liu HJ, Goh WP, Leung MY, Li YN, Norsten TB. Effect of nanoparticle stabilizing ligands and ligand-capped gold nanoparticles in polymer solar cells. *Sol Energy Mater Sol Cells* 2012;96:302–6.
- [130] Du P, Jing PT, Li D, Cao YH, Liu ZY, Sun ZC. Plasmonic Ag@oxide nanoprisms for enhanced performance of organic solar cells. *Small* 2015;11:2454–62.
- [131] Xie FX, Choy WCH, Wang CCD, Sha WEI, Fung DDS. Improving the efficiency of polymer solar cells by incorporating gold nanoparticles into all polymer layers. *Appl Phys Lett* 2011;99:153304.
- [132] Fung DDS, Qiao LF, Choy WCH, et al. Optical and electrical properties of efficiency enhanced polymer solar cells with Au nanoparticles in a PEDOT-PSS layer. *J Mater Chem* 2011;21:16349–56.
- [133] Baek S-W, Noh J, Lee C-H, Kim B, Seo M-K, Lee J-Y. Plasmonic forward scattering effect in organic solar cells: a powerful optical engineering method. *Sci Rep* 2013;3:1726.
- [134] Kim K, Jung B, Kim J, Kim W. Effects of embedding non-absorbing nanoparticles in organic photovoltaics on power conversion efficiency. *Sol Energy Mater Sol Cells* 2010;94:1835–9.
- [135] Lin W-K, Su S-H, Ma C-K, Yokoyama M. Enhancing conversion efficiency of inverted organic solar cells using Ag nanoparticles and long wavelength absorbing tin (II) phthalocyanine. *Org Electron* 2016;29:94–8.
- [136] Segal-Peretz T, Sorias O, Moshonov M, Deckman I, Orenstein M, Frey GL. Plasmonic nanoparticle incorporation into inverted hybrid organic-inorganic solar cells. *Org Electron* 2015;23:144–50.
- [137] Jung K, Song H-J, Lee G, et al. Plasmonic organic solar cells employing nanobump assembly via aerosol-derived nanoparticles. *Acs Nano* 2014;8:2590–601.
- [138] Cheng P-P, Ma G-F, Li J, et al. Plasmonic backscattering enhancement for inverted polymer solar cells. *J Mater Chem* 2012;22:22781–7.
- [139] Liu F, Nunzi J-M. Enhanced organic light emitting diode and solar cell performances using silver nano-clusters. *Org Electron* 2012;13:1623–32.
- [140] Beck FJ, Mokkapati S, Polman A, Catchpole KR. Asymmetry in photocurrent enhancement by plasmonic nanoparticle arrays located on the front or on the rear of solar cells. *Appl Phys Lett* 2010;96:033113.
- [141] Kakavelakis G, Vangelidis I, Heuer-Jungemann A, et al. Plasmonic backscattering effect in high-efficient organic photovoltaic devices. *Adv Energy Mater* 2016;6:1501640.
- [142] Bi YG, Feng J, Li YF, et al. Enhanced efficiency of organic light-emitting devices with metallic electrodes by integrating periodically corrugated structure. *Appl Phys Lett* 2012;100:053304.
- [143] Yates CJ, Samuel IDW, Burn PL, Wedge S, Barnes WL. Surface plasmon-polariton mediated emission from phosphorescent dendrimer light-emitting diodes. *Appl Phys Lett* 2006;88:161105.

- [144] Gu Y, Zhang DD, Ou QD, et al. Light extraction enhancement in organic light-emitting diodes based on localized surface plasmon and light scattering double-effect. *J Mater Chem C* 2013;1:4319–26.
- [145] Lee YH, Lee TK, Song I, et al. Boosting the performance of organic optoelectronic devices using multiple-patterned plasmonic nanostructures. *Adv Mater* 2016;28:4976–82.
- [146] Sha WEI, Choy WCH, Liu YG, Chew WC. Near-field multiple scattering effects of plasmonic nanospheres embedded into thin-film organic solar cells. *Appl Phys Lett* 2011;99:113304.
- [147] Li XH, Ren XG, Xie FX, et al. High-performance organic solar cells with broadband absorption enhancement and reliable reproducibility enabled by collective plasmonic effects. *Adv Optical, Mater* 2015;3:1220–31.
- [148] Song HM, Guo LQ, Liu ZJ, et al. Nanocavity enhancement for ultra-thin film optical absorber. *Adv Mater* 2014;26:2737–43.
- [149] Shen L, Yu WJ, Long YB, et al. Performance improvement of low-band-gap polymer solar cells by optical microcavity effect. *IEEE Electron Device Lett* 2013;34:87–9.
- [150] Wang Q, Xie Y, Soltani-Kordshuli F, Eslamian M. Progress in emerging solution-processed thin film solar cells – part I: polymer solar cells. *Renew Sust Energy Rev* 2016;56:347–61.
- [151] Lee YE, Kim SY, Jeong WI, Kim JJ. Microcavity tandem solar cells with a short circuit current higher than single cells. *Sol Energy Mater Sol Cells* 2013;114:59–64.
- [152] Chen K-S, Yip H-L, Salinas J-F, Xu Y-X, Chueh C-C, Jen AKY. Strong photocurrent enhancements in highly efficient flexible organic solar cells by adopting a microcavity configuration. *Adv Mater* 2014;26:3349–54.
- [153] Sergeant NP, Hadipour A, Niesen B, et al. Design of transparent anodes for resonant cavity enhanced light harvesting in organic solar cells. *Adv Mater* 2012;24:728–32.
- [154] Yu WJ, Shen L, Meng FX, Long YB, Ruan SP, Chen WY. Effects of the optical microcavity on the performance of ITO-free polymer solar cells with WO<sub>3</sub>/Ag/WO<sub>3</sub> transparent electrode. *Sol Energy Mater Sol Cells* 2012;100:226–30.
- [155] Zhang C, Zhao D, Gu D, et al. An ultrathin, smooth, and low-loss Al-doped Ag film and its application as a transparent electrode in organic photovoltaics. *Adv Mater* 2014;26:5696–701.
- [156] Kang H, Jung S, Jeong S, Kim G, Lee K. Polymer-metal hybrid transparent electrodes for flexible electronics. *Nat Commun* 2015;6:6503.
- [157] Fortunato E, Ginley D, Hosono H, Paine DC. Transparent conducting oxides for photovoltaics. *Mrs Bulletin* 2007;32:242–7.
- [158] Ou XL, Xu M, Feng J, Sun HB. Flexible and efficient ITO-free semitransparent perovskite solar cells. *Sol Energy Mater Sol Cells* 2016;157:660–5.
- [159] Ma R, Feng J, Yin D, Sun H-B. Highly efficient and mechanically robust stretchable polymer solar cells with random buckling. *Org Electron* 2017;43:77–81.
- [160] Bi Y-G, Feng J, Ji J-H, et al. Ultrathin and ultrasoft Au films as transparent electrodes in ITO-free organic light-emitting devices. *Nanoscale* 2016;8:10010–5.
- [161] Huang J, Li C-Z, Chueh C-C, Liu S-Q, Yu J-S, Jen AKY. 10.4% Power conversion efficiency of ITO-free organic photovoltaics through enhanced light trapping configuration. *Adv Energy Mater* 2015;5:1500406.
- [162] Salinas J-F, Yip H-L, Chueh C-C, Li C-Z, Maldonado J-L, Jen AKY. Optical design of transparent thin metal electrodes to enhance in-coupling and trapping of light in flexible polymer solar cells. *Adv Mater* 2012;24:6362–7.
- [163] Lin H-W, Chiu S-W, Lin L-Y, et al. Device engineering for highly efficient top-illuminated organic solar cells with microcavity structures. *Adv Mater* 2012;24:2269–72.
- [164] New E, Howells T, Sullivan P, Jones TS. Small molecule tandem organic photovoltaic cells incorporating an alpha-NPD optical spacer layer. *Org Electron* 2013;14:2353–9.
- [165] Chan MY, Lai SL, Lau KM, Lee CS, Lee ST. Application of metal-doped organic layer both as exciton blocker and optical spacer for organic photovoltaic devices. *Appl Phys Lett* 2006;89:163515.
- [166] Vervisch W, Riviere G, Vedraïne S, et al. Optical-electrical simulation of organic solar cells: influence of light trapping by photonic crystal and ZnO spacer on electrical characteristics. *J Appl Phys* 2012;111:094506.
- [167] Peumans P, Bulović V, Forrest SR. Efficient photon harvesting at high optical intensities in ultrathin organic double-heterostructure photovoltaic diodes. *Appl Phys Lett* 2000;76:2650–2.
- [168] Kim JY, Kim SH, Lee HH, et al. New architecture for high-efficiency polymer photovoltaic cells using solution-based titanium oxide as an optical spacer. *Adv Mater* 2006;18:572–6.
- [169] Timofeev IV, Pankin PS, Vetrov SY, Arkhipkin VG, Lee W, Zyryanov VY. Chiral optical Tamm states: temporal coupled-mode theory. *Crystals* 2017;7:113.
- [170] Zhang XL, Song JF, Li XB, Feng J, Sun HB. Strongly localized evanescent optical Tamm states at metal-DBR interface. *J Lightwave Technol* 2013;31:1654–9.
- [171] Kivshar YS. Nonlinear Tamm states and surface effects in periodic photonic structures. *Laser Phys Lett* 2008;5:703–13.
- [172] Zhang X-L, Song J-F, Li X-B, Feng J, Sun H-B. Optical Tamm states enhanced broad-band absorption of organic solar cells. *Appl Phys Lett* 2012;101:243901.
- [173] Zhang XL, Song JF, Li XB, Feng J, Sun HB. Light trapping schemes in organic solar cells: a comparison between optical Tamm states and Fabry-Perot cavity modes. *Org Electron* 2013;14:1577–85.
- [174] Zhang DD, Jiang XC, Wang R, et al. Enhanced performance of semitransparent inverted organic photovoltaic devices via a high reflector structure. *ACS Appl Mater Interfaces* 2013;5:10185–90.
- [175] Yusoff AB, Lee SJ, Kim HP, Shneider FK, da Silva WJ, Jang J. 8.91% power conversion efficiency for polymer tandem solar cells. *Adv Funct Mater* 2014;24:2240–7.
- [176] Yang J, You JB, Chen CC, et al. Plasmonic polymer tandem solar cell. *Acs Nano* 2011;5:6210–7.
- [177] Gilot J, Wienk MM, Janssen RAJ. Optimizing polymer tandem solar cells. *Adv Mater* 2010;22:E67–71.
- [178] Dou L, You J, Yang J, et al. Tandem polymer solar cells featuring a spectrally matched low-bandgap polymer. *Nat Photon* 2012;6:180–5.
- [179] Jin Y, Feng J, Xu M, et al. Matching photocurrents of sub-cells in double-junction organic solar cells via coupling between surface plasmon polaritons and microcavity modes. *Adv Opt Mater* 2013;1:809–13.
- [180] Jin Y, Feng J, Zhang XL, et al. Broadband absorption enhancement in organic solar cells with an antenna layer through surface-plasmon mediated energy transfer. *Appl Phys Lett* 2015;106:223303.